

Identification of GSK3186899/DDD853651 as a Preclinical Development Candidate for the Treatment of Visceral Leishmaniasis

Michael G. Thomas,[†] Manu De Rycker,[†] Myriam Ajakane,[‡] Sébastien Albrecht,[†] Ana Isabel Álvarez-Pedraglio,[§] Markus Boesche,[‡] Stephen Brand,[†] Lorna Campbell,[†] Juan Cantizani-Perez,[§] Laura A.T. Cleghorn,[†] Royston C.B. Copley,^{||} Sabrina D. Crouch,[§] Alain Daugan,[⊥] Gerard Drewes,[‡] Santiago Ferrer,[§] Sonja Ghidelli-Disse,[‡] Silvia Gonzalez,[§] Stephanie L. Gresham,[#] Alan P. Hill,^{||} Sean J. Hindley,^{||} Rhiannon M. Lowe,[#] Claire J. MacKenzie,[†] Lorna MacLean,[†] Sujatha Manthri,[†] Franck Martin,[⊥] Juan Miguel-Siles,[§] Van Loc Nguyen,[⊥] Suzanne Norval,[†] Maria Osuna-Cabello,[†] Andrew Woodland,[†] Stephen Patterson,[†] Imanol Pena,[§] Maria Teresa Quesada-Campos,[§] Iain H. Reid,^{||} Charlotte Reville,[†] Jennifer Riley,[†] Jose Ramon Ruiz-Gomez,[§] Yoko Shishikura,[†] Frederick R.C. Simeons,[†] Alasdair Smith,[†] Victoria C. Smith,[†] Daniel Spinks,[†] Laste Stojanovski,[†] John Thomas,[†] Stephen Thompson,[†] Tim Underwood,^{||} David W. Gray,[†] Jose M. Fiandor,[§] Ian H. Gilbert,[†] Paul G. Wyatt,^{*,†} Kevin D. Read,^{*,†} and Timothy J. Miles^{*,§}

[†]Drug Discovery Unit, Wellcome Centre for Anti-Infectives Research, Division of Biological Chemistry and Drug Discovery, School of Life Sciences, University of Dundee, Dundee DD1 5EH, U.K.

[‡]Cellzome GmbH, A GlaxoSmithKline Company, Meyerhofstrasse 1, 69117 Heidelberg, Germany

[§]Global Health R&D, GlaxoSmithKline, Calle Severo Ochoa, 2, 28760 Tres Cantos, Madrid Spain

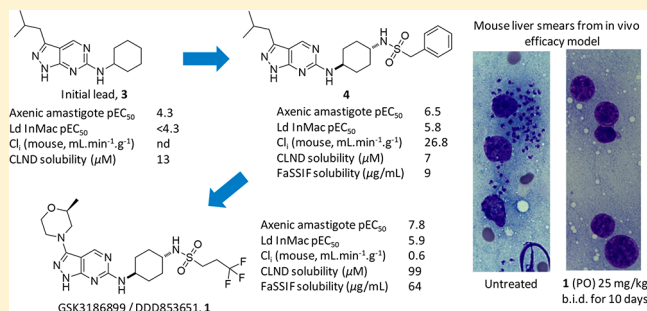
^{||}Platform Technology & Science, GlaxoSmithKline Medicines Research Centre, Gunnels Wood Road, Stevenage, Hertfordshire SG1 2NY, U.K.

[⊥]Centre de Recherche, GlaxoSmithKline, Les Ulis, 25,27 Avenue du Québec, 91140 Villebon sur Yvette France

[#]Platform Technology & Science, GlaxoSmithKline, David Jack Centre for R&D, Park Road, Ware, Hertfordshire SG12 0DP, U.K.

Supporting Information

ABSTRACT: The leishmaniasis are diseases that affect millions of people across the world, in particular visceral leishmaniasis (VL) which is fatal unless treated. Current standard of care for VL suffers from multiple issues and there is a limited pipeline of new candidate drugs. As such, there is a clear unmet medical need to identify new treatments. This paper describes the optimization of a phenotypic hit against *Leishmania donovani*, the major causative organism of VL. The key challenges were to balance solubility and metabolic stability while maintaining potency. Herein, strategies to address these shortcomings and enhance efficacy are discussed, culminating in the discovery of preclinical development candidate GSK3186899/DDD853651 (1) for VL.



INTRODUCTION

Kinetoplastid diseases are part of the list of the neglected tropical diseases (NTDs) as defined by the World Health Organisation (WHO).¹ These diseases are caused by a group of flagellated protozoans that are characterized by the presence of a distinct network of DNA (known as “kinetoplast”) in their single large mitochondrion.² The human diseases more commonly caused by these parasites include, among others, various forms of leishmaniasis (cutaneous, muco-cutaneous, and visceral). These diseases affect millions of people, not only those infected, but

also the communities in which they live, contributing to a perpetual cycle of poverty. The leishmaniasis affect people across Africa, the Middle East, South America, and Asia. There are about 20 species or subspecies of *Leishmania* which cause human disease. Visceral leishmaniasis (VL, also known as kala azar), caused by *Leishmania donovani* and *Leishmania infantum*, is typically fatal without treatment with 200000–400000 new

Received: August 2, 2018

Published: December 20, 2018

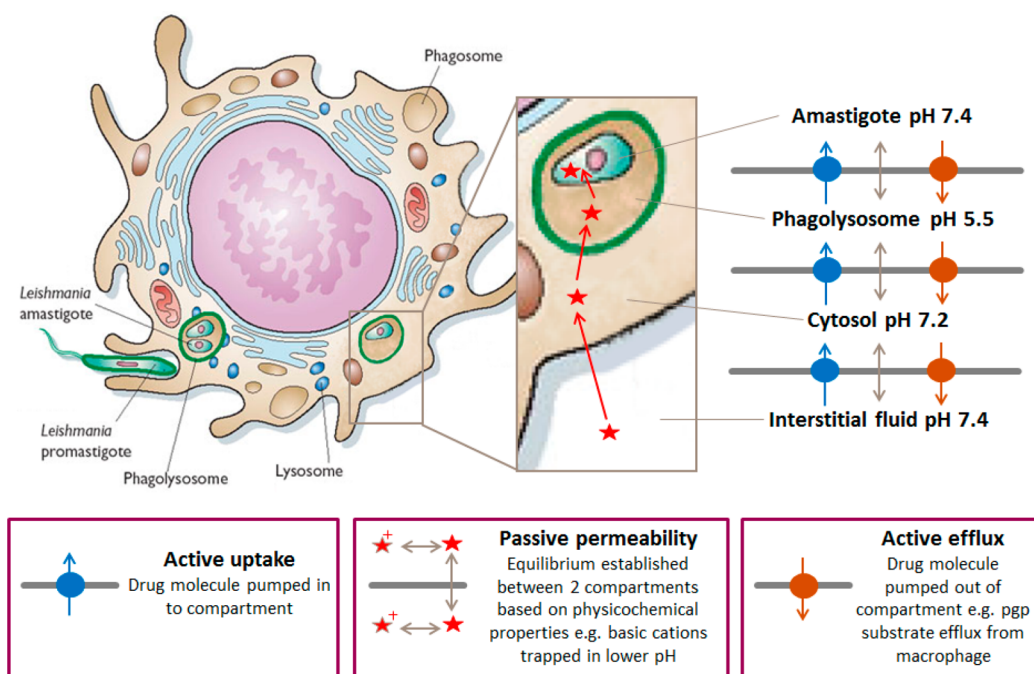


Figure 1. Reaching the biophase for visceral leishmania within macrophages. Reprinted (adapted) with permission from ref 47. Copyright 2002 Nature Publishing Group.

cases each year and approximately 20000–30000 deaths.³ Current therapies are not fit for use in resource-poor settings due to a combination of issues such as difficult administration, length of treatment, side effects, teratogenicity, cost, resistance, and/or clinical relapse.^{4–7} At the time of this work, the external development pipeline for VL was sparse with only two additional new chemical entities (NCEs) just entering the early preclinical phase.⁸ Therefore, there was a clear unmet medical need for a new therapeutic class.

The primary objective of a collaboration between the Drug Discovery Unit, University of Dundee and GSK (funded by Wellcome), has been to identify safe, effective, oral, and short-course (ideally ≤ 10 days) drug candidates for VL, in line with the DNDi (Drugs for Neglected Disease *initiative*) target product profile.⁹ Hence, the focus was to identify orally available compounds that demonstrate both *in vitro* and *in vivo* parasite suppression comparable to miltefosine (the only available oral therapy) in preclinical models, with an appropriate safety profile. This strategy of focusing on parasite suppression has been used successfully for discovery of most of the current protozoan chemotherapies.¹⁰ Because there are very few fully validated druggable targets in the kinetoplastids, most groups have focused on phenotypic approaches.^{11,12}

Leishmania parasites have a complex life cycle, involving a vector (sandfly) stage and a host (human) stage.¹³ Given the differences in biology between the vector and the host stage, it is important that compounds are screened against the correct physiological stage (amastigotes). In the human host, the parasites are found within macrophages, more specifically within parasitophorous vacuoles where the pH is ~ 5.5 . A high-content screening method for this stage was recently developed, where the parasites are cultured in differentiated THP-1 cells, representative of the human disease.¹⁴ In the experience of this collaboration and others,¹⁵ the hit rate was very low using this whole cell *in vitro* intracellular amastigote assay, which may be for several reasons. First, the parasites are dividing relatively

slowly in this assay, and second, compounds need to cross three membranes and navigate two changes in pH to demonstrate *in vitro* potency (Figure 1). However, the assay only identifies cytotoxic, rather than cytostatic compounds, which is an important consideration when identifying new compound series. Notably, all compounds which are either in the clinic, or in clinical development, exhibit activity in this assay.¹⁴

This publication details the lead optimization of a *N1*-(1*H*-pyrazolo[3,4-*d*]pyrimidin-6-yl)cyclohexyl-1,4-*trans*-diamine series to find an appropriate balance between potency, relevant measures of solubility, and/or metabolic stability. This effort led to the *in vivo* profiling of a number of analogues, and finally the identification of precandidate asset GSK3186899/DDD853651, **1** (Figure 2).^{16,17} Subsequent target deconvolution identified that the principal target was Cdc2-related kinase 12 (CRK12),¹⁷ although this was unknown during the lead optimization program.

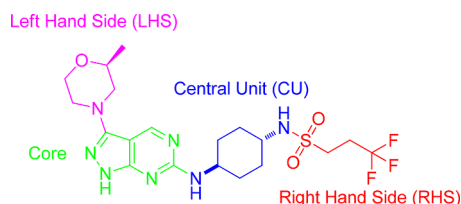
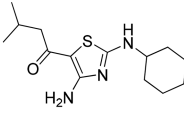
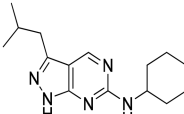
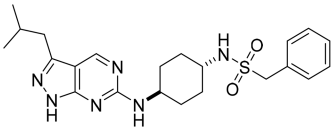
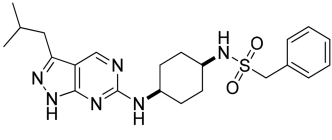


Figure 2. Structure of GSK3186899/DDD853651, **1**.

RESULTS AND DISCUSSION

We previously reported that diaminothiazole **2** demonstrated activity against the related parasite *Trypanosoma brucei*,¹⁸ and that a scaffold-hopping strategy identified pyrazolopyrimidine **3** as having very weak activity against *L. donovani* (Ld) axenic amastigotes,¹⁷ albeit with no activity against intracellular parasites. Several changes were made to the cyclohexyl ring of **3** to allow us to explore the SAR around this portion of the

Table 1. In Vitro Profile of 2–4

Compound	Axenic amastigote (pEC ₅₀) ¹⁷	Ld InMac (pEC ₅₀) ^a / THP-1 (pEC ₅₀)	Cl _i (mouse liver microsomes, mL·min ⁻¹ ·g ⁻¹) ^b
 2	4.3	nd	18.7
 3	4.5	<4.3 / <4.3	nd
 4-trans	6.5	5.8 / <4.3	26.9
 4-cis	nd	4.7 / <4.3	nd

^aLd InMac is the intramacrophage assay carried out in THP-1 cells with *L. donovani* amastigotes.¹⁴ Data are the result of three replicates. ^bCl_i is mouse liver microsomal intrinsic clearance; nd is not determined.

molecule, and one such change, the introduction of a functionalized 4-amino group, led to compound **4-trans** with in vitro potency against intracellular parasites and no effect on the nondividing human host cells (THP-1) (Table 1). Interestingly **4-cis** was >10-fold less potent within the intramacrophage assay compared to **4-trans**. This relationship was general across the series, and as such, the *cis*-isomers will not be discussed further.

On the basis of the data presented in Table 1, the initial medicinal chemistry focus was to improve metabolic stability (mouse microsomal intrinsic clearance <5 mL·min⁻¹·g⁻¹), with the aim of rapidly identifying analogues suitable for testing in an in vivo mouse efficacy model. Despite the mode of action (MoA) of the series being unknown when the chemistry program was initiated, **3** and **4** did closely resemble a set of antitumor cyclin dependent kinase inhibitors.¹⁹ The closest exemplar was *N*-(*trans*-4-((3-(5-fluoro-2-methoxyphenyl)-1*H*-pyrazolo[3,4-*d*]pyrimidin-6-yl)amino)cyclohexyl)methanesulfonamide (example **26** from ref 19), which demonstrated IC₅₀ values of 0.199 and 0.114 μM against Cdk4 and Cdk2, respectively. Repurposing of human kinase inhibitors as a strategy for infectious and neglected diseases has been explored by others,^{20–22} in which they all recognize selectivity over the human orthologue as a potential challenge. Therefore, monitoring against a panel of human kinases for this series would be critical, particularly for compounds progressing into in vivo efficacy experiments.

Interestingly, replacements for the sulphonamide (e.g. **5**) were inactive against intracellular parasites within this series (Table 2). Exchanging the benzyl group with an *iso*-butyl group led to an increase in activity (**6**), although both compounds were metabolically unstable. Replacing the *iso*-butyl group (RHS) with a trifluoropropyl group (**7**) gave greater stability when incubated with mouse liver microsomes and only a small loss in potency compared to **6**. Switching focus to the LHS, it was noted that replacing the *iso*-butyl group with either a 2-methoxyphenyl or a 2-pyridyl caused a significant increase in potency (**8** and **9**), the latter being noteworthy for also having improved mouse metabolic stability. Additionally, this series demonstrated increased stability in human vs mouse liver microsomes (see **5** and **8** in Table 2).

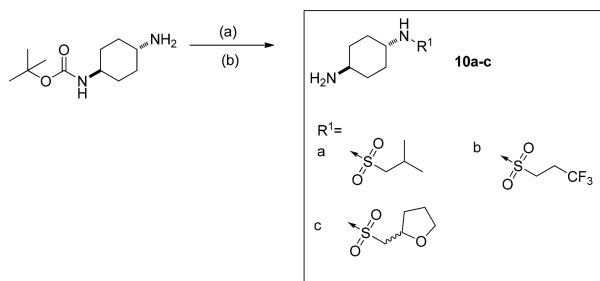
To facilitate the synthesis of the compounds described within this paper, a set of key amines was synthesized according to Scheme 1. *N*-Boc-*trans*-1,4-cyclohexanediamine was deprotected with *n*-BuLi then reacted with the relevant sulphonyl chloride, and the resulting Boc protected intermediates were treated with TFA to give **10a–c**.

Examples **3–9**, **15**, and **17** were synthesized according to Scheme 2. Thus, 5-bromo-2-chloro-4-methoxypyrimidine was treated with *iso*-propylmagnesium chloride and various aldehydes at –40 °C. The resulting alcohols were oxidized with Dess–Martin periodinane to yield ketones **11a–d**. Treatment of **11a** with cyclohexylamine in the presence of Hünig's base led to aminopyrimidine **12**. Similarly, **11a** was treated with *tert*-butyl-(*trans*-4-aminocyclohexyl)carbamate,

Table 2. In Vitro Profiles of 4–9

Compound	R ¹	R ²	Ld InMac (pEC ₅₀) ^a	THP-1 (pEC ₅₀) / HepG2 (pEC ₅₀) ^b	Cl _i (liver microsomes, mL·min ⁻¹ ·g ⁻¹) ^c
4-trans			5.8	<4.3 / <4	26.9 (mouse)
5			<4.3	<4.3 / 4.3	9.5 (mouse) 1.9 (human)
6			6.2	<4.3 / 4.2	17.2 (mouse)
7			5.9	<4.3 / 4.3	3.6 (mouse)
8			7.7	<4.3 / <4	48.0 (mouse) 14.1 (human)
9			7.1	4.3 / <4	2.1 (mouse)

^aLd InMac is the intramacrophage assay carried out in THP-1 cells with *L. donovani* amastigotes.¹⁴ Data are the result of at least four replicates.
^bHepG2 is a human liver cancer cell line. ^cCl_i is liver microsomal intrinsic clearance.

Scheme 1. Synthesis of Intermediates 10a–c^a

^aReagents and conditions: (a) *n*-BuLi, R¹Cl, THF, –78°C, 1–1.5 h; (b) TFA, DCM, RT, overnight, 80–99% over 2 steps

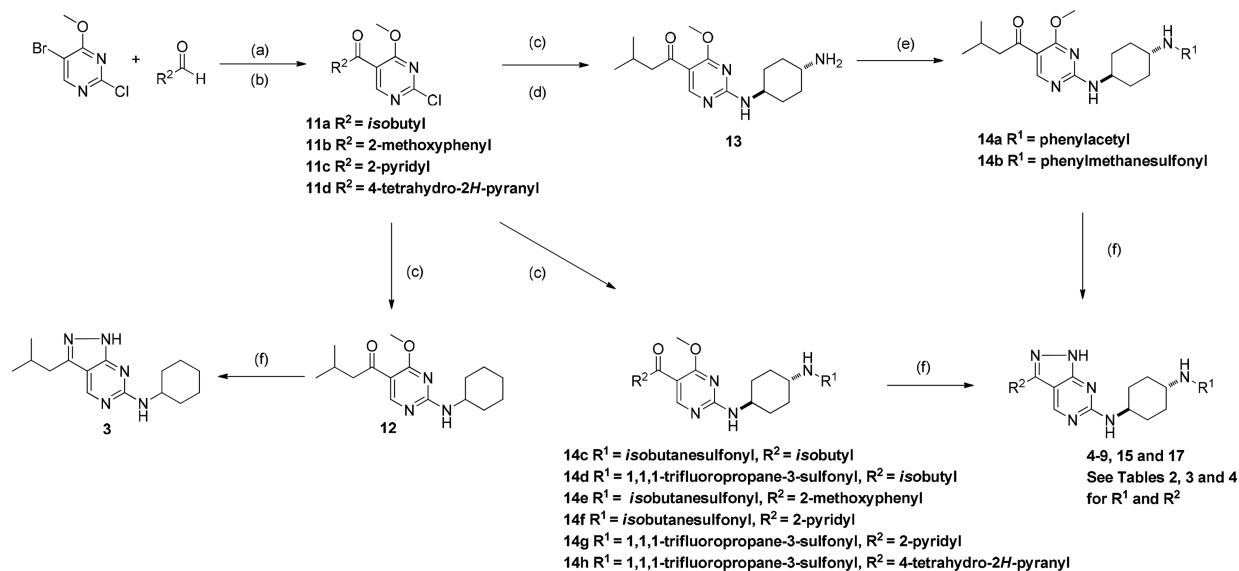
and the resulting compound treated with TFA to remove the Boc group, yielding **13**. This intermediate could then be either acylated or sulfonylated to give **14a,b**. Alternatively, a more direct route was used for synthesis of intermediates **14c–h**, whereby coupling of the appropriate combinations of **10a–c** with **11a–d** led to the relevant intermediates. Finally, treatment of either **12** or **14a–h** with hydrazine hydrate generated the desired target compounds (**3–9**, **15**, and **17**).

On the basis of the SAR learnings summarized in Table 2 (notably **7** and **9**), compound **15** was prepared with the aim of improving potency and metabolic stability over **4** (Table 3). The in vitro profile of **15** supported progression into a mouse pharmacokinetic (PK) study. However, the compound showed poor solubility when measured using chemiluminescent nitrogen detection (CLND), a technique used to measure kinetic aqueous solubility.²³ It would therefore be necessary to use a

highly solubilizing vehicle (10% (v/v) dimethyl sulfoxide (DMSO), 60% polyethylene glycol 400, and 30% deionized water) to maximize the chance of achieving sufficient exposure in mice when **15** was progressed to in vivo experiments.

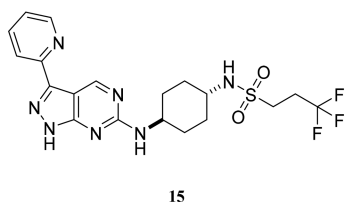
To monitor the effects of the series on human kinases, chemoproteomic profiling on Kinobeads was performed in a K-562 protein extract to identify potential human off-targets for **8** and **15** (Figure 3). The compounds were tested at a concentration of 5 μM for their activity against 210 human protein kinases, and while **8** showed competition of several protein kinases, **15** did not affect any of the captured protein kinases. This gave us confidence that a suitable kinase selectivity profile could be achieved within this series. On the basis of this observation and overall in vitro/DMPK profile (Table 3), **15** was progressed to an animal disease model for VL.

There are a number of preclinical in vivo animal protocols available for assessing the efficacy of compounds intended to treat VL, including mouse, rat, hamster, dog, and monkey models.²⁴ Of these, mouse and hamster are the most common models for testing drug efficacy.^{25,26} However, there is a marked lack of clinical validation of these models and the absence of clinical Pharmacokinetic/Pharmacodynamic (PK/PD) data makes it impossible to suggest which model is more predictive of the clinical outcome in human. That said, after reviewing the available clinical data^{27,28} and comparing to our nonclinical in vivo data for miltefosine, it was observed that the mouse exposure data was predictive for humans. In addition, both liposomal amphotericin B and miltefosine achieve a >95% suppression in parasite load within this mouse model.²⁶ Mouse was therefore selected as our primary model to evaluate in vivo efficacy.

Scheme 2. Synthesis of Compounds 3–9, 15, and 17^a

^aReagents and conditions: (a) *i*PrMgCl (2M in Et₂O), THF, -40 °C, 30 min; (b) Dess–Martin periodinane, DCM, RT, 1 h, 39–67% over two steps; (c) cyclohexylamine (for 12), *tert*-butyl-(*trans*-4-aminocyclohexyl)carbamate (for 13) or 10a–c (for 14c–h), DIPEA, EtOH, 120 °C (microwave, 2 h); (d) TFA, DCM, 1 h, 80% over two steps; (e) phenylacetyl chloride, trimethylamine, DCM, overnight (for 14a), benzylsulphonyl chloride, Cs₂CO₃, DMF, overnight (for 14b); (f) hydrazine hydrate, EtOH, 150 °C (microwave), 30 min to 1 h, 30–72% over two steps.

Table 3. In Vitro Profile of 15



Ld InMac (pEC ₅₀) ^a	6.3
THP-1 (pEC ₅₀) / HepG2 (pEC ₅₀) ^b	4.3 / <4
Cl _i (mL·min ⁻¹ ·g ⁻¹) ^c	0.6 (mouse), <0.5 (human)
CLND solubility (μM) ^d	8
Plasma protein binding (% unbound)	13% (mouse), 8% (human)
Oral PK profile at 10 mg/kg in female Balb/c mice (n=3)	
AUC _{0–last} (ng·hr·mL ⁻¹) ^e	17358 (%CV = 79) ^f
C _{max} (ng·mL ⁻¹) ^g	1910
Cl _b (mL·min ⁻¹ ·kg ⁻¹) ^h	4
V _{ss} (L·kg) ⁱ	0.9
F _{po} (%) ^j	44

^aLd InMac is the intramacrophage assay carried out in THP-1 cells with *L. donovani* amastigotes.¹⁴ Data are the result of 18 replicates. ^bHepG2 is a human liver cancer cell line. ^cCl_i is liver microsomal intrinsic clearance. ^dCLND is kinetic aqueous solubility measured using chemiluminescent nitrogen detection.²³ ^eAUC_{0–last} is the area under the curve until the last measurement. ^f%CV is the % of coefficient of variation. ^gC_{max} is the maximum concentration reached. ^hCl_b is mouse clearance in blood. ⁱV_{ss} is volume of distribution at steady state. ^jF_{po} is oral bioavailability.

Female Balb/c mice were infected with *L. donovani* amastigotes, and the infection was allowed to establish for 7 days. These mice (groups of 5) were treated with either vehicle (oral), sodium stibogluconate (pentostam, 15 mg/kg, which is the ED₃₀, subcutaneously), miltefosine (12 mg/kg, which is the ED₇₀, orally) as standards, or 15 (50 mg/kg, orally). Pentosam and miltefosine were dosed once daily for 5 days with vehicle and 15 dosed twice daily over same period.

Fourteen days, after infection, all animals were humanely euthanized and parasite burden was determined microscopically.²⁹ Parasite burden was expressed in Leishman–Donovan units (LDU), the number of amastigotes per 500 nucleated cells multiplied by the organ weight in grammes.³⁰

Pleasingly, 15 demonstrated an 85% suppression in parasite load (Figure 4) within the liver with 50 mg/kg b.i.d. dosing for 5 days, while the controls performed as expected. This result established excellent proof of concept for the series. Despite 15 demonstrating promising efficacy and oral bioavailability (44%), marked variability in exposure was observed (%CV = 79, Table

3) and it was also noted that first pass metabolism could only account for 3% of the remaining noncirculating parent compound (56%). Because 15 had a high artificial membrane permeability (4.4×10^{-5} cm/s) and low CLND solubility (Table 3), it was hypothesized that increasing the solubility should increase exposure and reduce variability.

The property forecast index (PFI) provides a probabilistic score of the likely developability risks and solubility of compounds.³¹ 15 had a PFI of 7.2 and the impact of modulating PFI by either introducing polarity (reducing ChroMLogD) or incorporating saturated isosteres (reducing ~ #Ar) are highlighted in Table 4. A collateral benefit of reducing the PFI was that 15 and subsequent molecules all displayed excellent metabolic stability.

16 was synthesized according to Scheme 3, where commercially available 3-bromo-6-(methylthio)-1H-pyrazolo-[3,4-*d*] pyrimidine was oxidized to sulphone 22. The pyrazole N–H of 22 was then protected with THP to yield 23, and the sulphone was subsequently displaced with 10b. The resulting

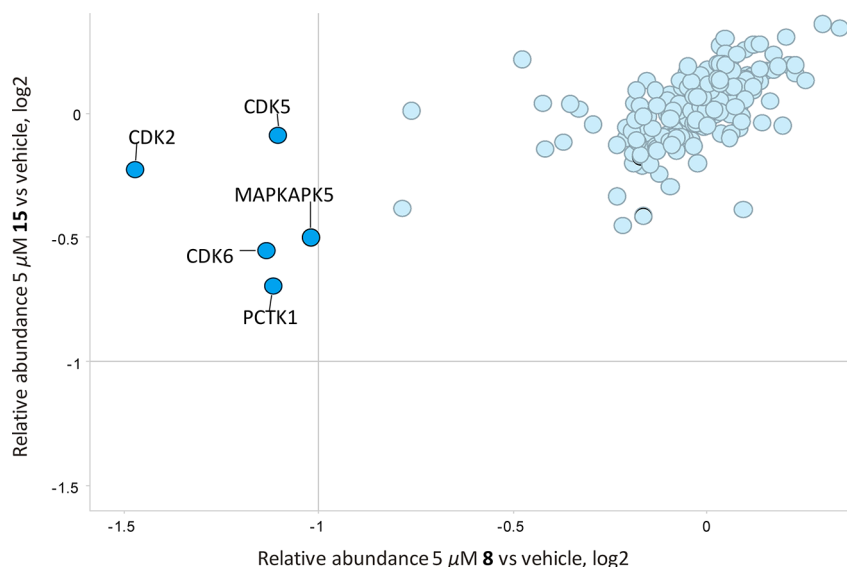


Figure 3. Chemoproteomic affinity profiling of compounds **8** and **15**. Kinobeads were incubated with K-562 cell extract either in the presence of vehicle (DMSO) or compound **15** or compound **8** ($5 \mu\text{M}$). Proteins captured by the beads in both conditions were quantified by LC–MS/MS analysis. Labeled proteins show more than 2-fold reduced binding to the Kinobead matrix due to competition with compounds **15** or **8** against vehicle respectively and represent potential human off-targets.

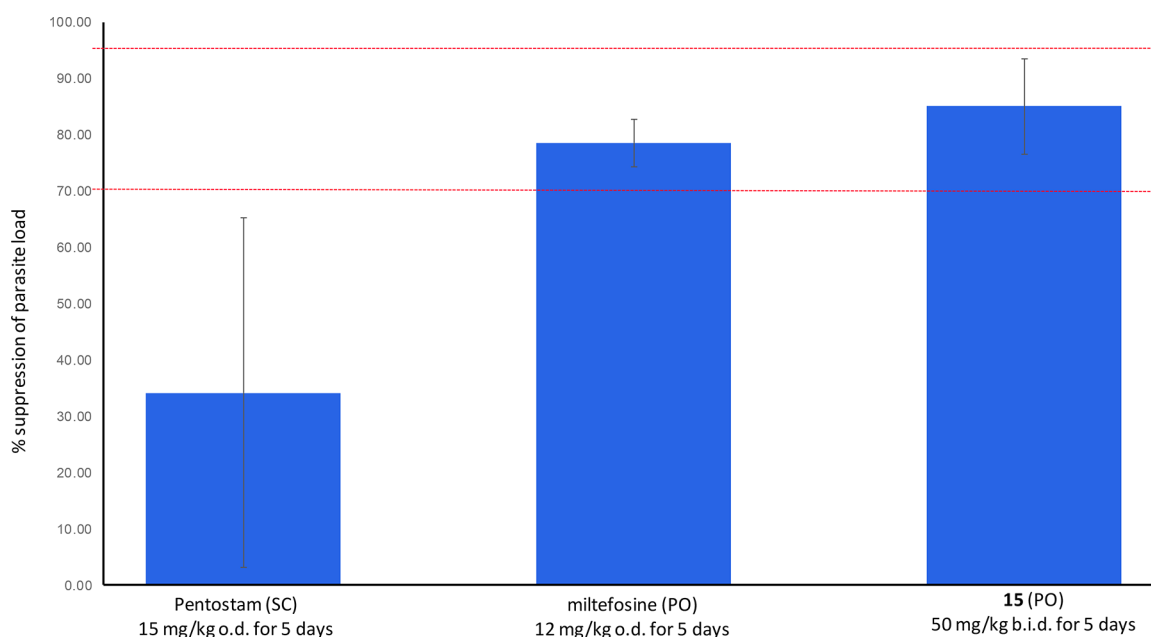


Figure 4. In vivo efficacy profile of pentostam, miltefosine, and **15**. The mean LDU values from individual animal livers were compared to the control to give the percentage (%) suppression of parasite load in Balb/c mice (that were infected with *L. donovani*). Error bars represent the standard deviation (SD). Lead optimization criteria was 70% suppression in liver parasite burden, while preclinical candidate was >95%.

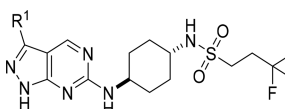
bromide **24** was reacted with 5-pyrimidylboronic acid using Suzuki coupling conditions, and subsequent THP deprotection led to **16**.

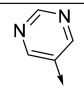
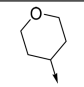
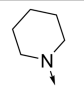
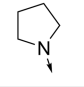
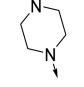
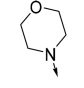
17 was synthesized according to Scheme 2, whereas an alternative route was required for compounds **18–21**. Synthesis of these derivatives, along with **1** and **36–38**, was accomplished according to Scheme 4. Commercially available 2,4-dichloro-5-pyrimidinecarbonyl chloride was treated with a suitable amine to give amides **26a–g**, which were subsequently treated with sodium methoxide to selectively displace the pyrimidinyl 4-chloro yielding **27a–g**. The pyrimidinyl 2-chloro group could then be displaced with amine **10a** or **10b** to give **28a–g**. Finally, reaction of **28a–g** with Lawesson's reagent followed by

treatment with hydrazine gave compounds **1**, **18–21**, and **36–38**. In the case of **29f**, the Boc group was deprotected with TFA following the reaction with hydrazine to give **20**. Chiral separation of **29c** furnished the enantiomers **36** and **37**.

Several LHS heteroaromatic analogues were synthesized. However, as demonstrated by **16**, none showed any advantage over **15** in terms of either solubility or potency (Table 4). Hence, the focus was to identify saturated isosteres to replace the pyridyl LHS in **15**, thus reducing the number of aromatic rings. Initial compounds **17** and **18**, where the pyridyl was replaced by a saturated ring to reduce PFI, showed an improvement in solubility, although both were less potent than **15**. Pyrrolidine **19** demonstrated similar in vitro potency to piperidine **18**, albeit

Table 4. PFI and in Vitro Profiles of 16–21



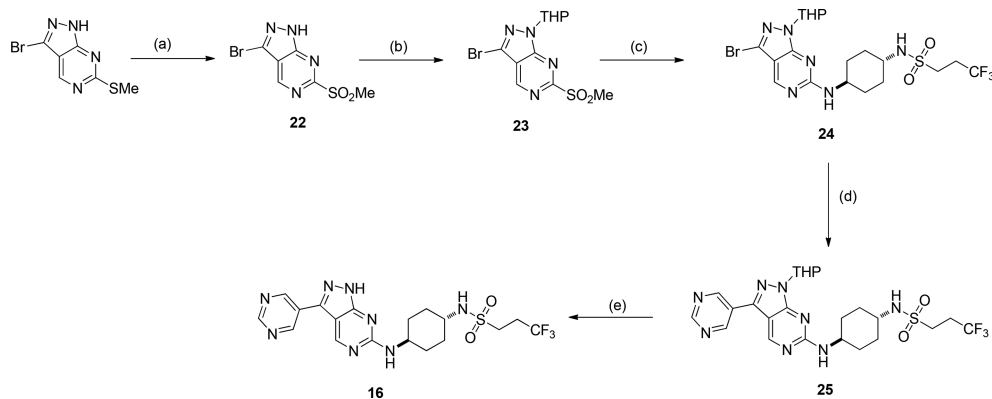
Compound	R ¹	Ld InMac (pEC ₅₀) ^a	Solubility (CLND, μM) ^b	PFI ^c	Chrom LogD _{pH7.4} ^d / no. of Ar
16		5.2	11	6.0	3.0 / 3
17		5.5	35	5.2	3.2 / 2
18		5.8	46	6.4	4.4 / 2
19		5.7	12	6.0	4.0 / 2
20		4.5	346	3.6	1.6 / 2
21		5.5	259	5.0	3.0 / 2

^aLd InMac is the intramacrophage assay carried out in THP-1 cells with *L. donovani* amastigotes.¹⁴ Data are the result of at least three replicates.

^bCLND is kinetic aqueous solubility measured using chemiluminescent nitrogen detection.²³ ^cPFI is the property forecast index.³¹

^dChromLogD_{pH7.4} is a measure lipophilicity at pH7.4.³¹

Scheme 3. Synthesis of Compound 16⁴⁴

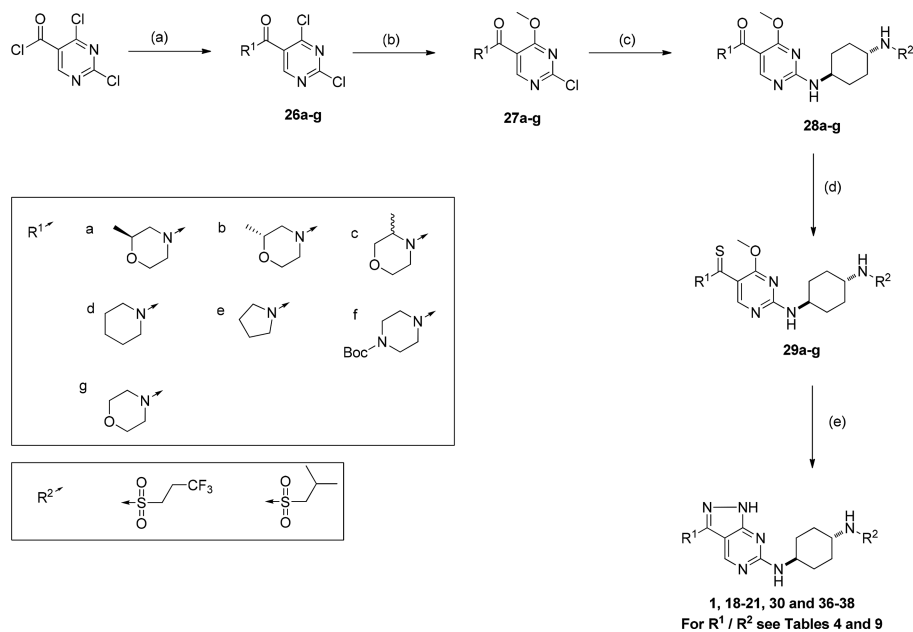


⁴⁴Reagents and conditions: (a) oxone, MeCN, H₂O, RT, 3 h, 62%; (b) 3,4-dihydro-2H-pyran, *p*-toluenesulfonic acid monohydrate, THF, reflux, overnight, 79%; (c) **10b**, DIPEA, EtOH, 100°C, overnight, 68%; (d) Pd(PPh₃)₄, K₂CO₃, DMF, H₂O, 150°C, 20 min; (e) conc HCl, MeOH, 100°C, 30 min, 85% over two steps.

lower solubility. Interestingly, piperazine **20** was less potent but had excellent CLND solubility, presumably due to increased basicity and reduced ChromLogD. Interrogation of the data (Figure 5) suggested targeting a PFI between 4.2 and 6 would give a high probability of achieving a desirable CLND solubility while maintaining intracellular potency and good absorption.

Promisingly, the morpholine analogue **21** in Table 4 showed similar in vitro potency to piperidine **18** with reduced PFI and

increased CLND solubility. Knowing that an improvement in potency (in vitro) between compounds **9** and **15** was observed, the *iso*-butyl-sulphonamide version of morpholine analogue **21** was of interest. This compound (**30**) was synthesized following Scheme 4, i.e., displacing the chloro of **27g** with amine **10a**. As shown in Table 5, **30** demonstrated excellent in vitro potency and CLND solubility, additionally showing a similar profile to

Scheme 4. Synthesis of Compounds 1, 18–21, 30, and 36–38^a

^aReagents and conditions: (a) $R^1\text{H}$, DIPEA, DCM, 0°C, 3 h, 53–92%; (b) NaOMe, THF, –40°C, 3 h, 48–86%; (c) 10a or 10b, DIPEA, 1,4-dioxane, 100°C, overnight, 54–71%; (d) Lawesson's reagent, THF, 45°C, 2 h; (e) hydrazine hydrate, 1,4-dioxane, 90 °C, overnight, 47–58% over two steps.

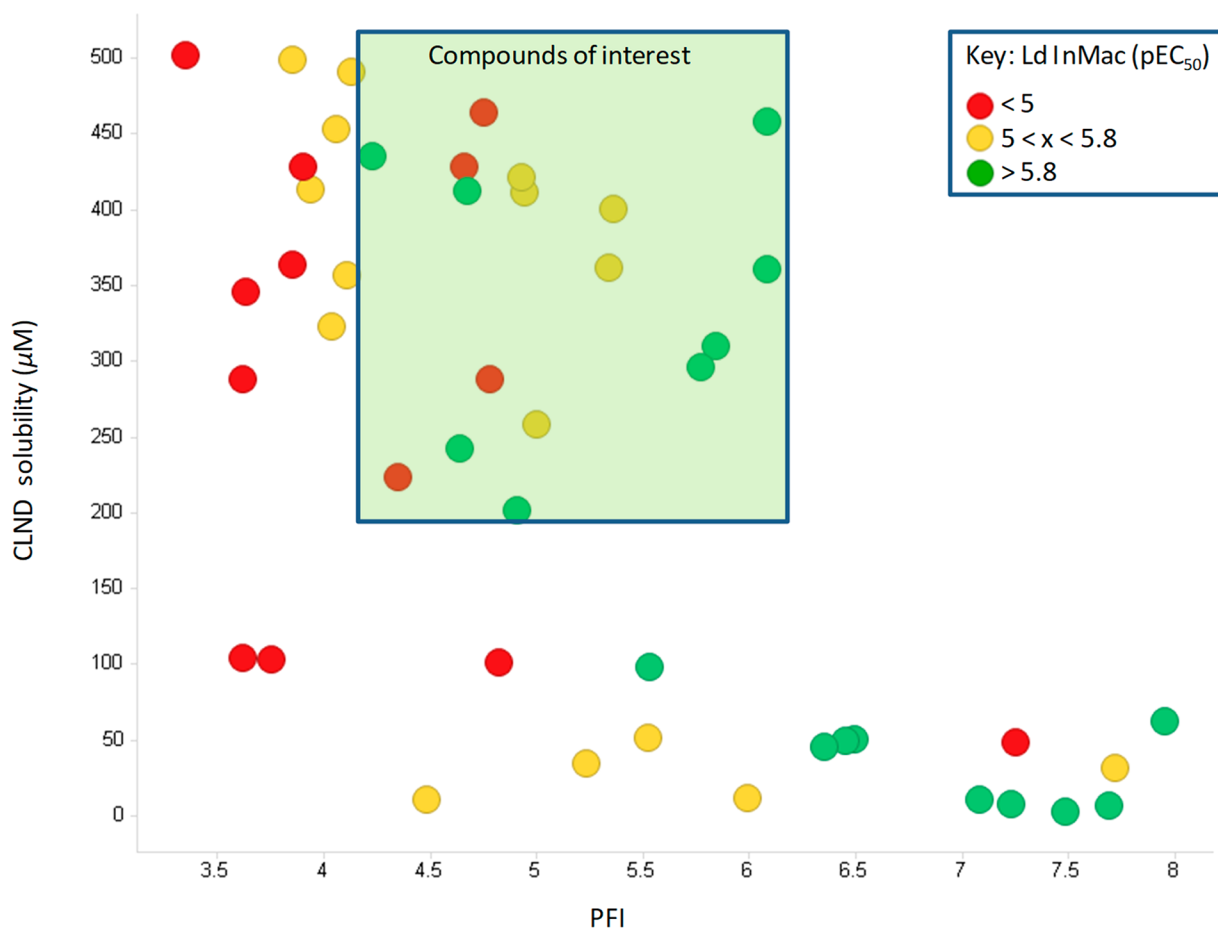
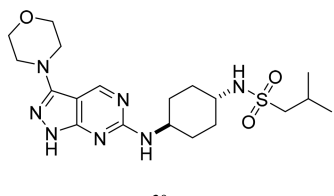


Figure 5. CLND solubility vs PFI profile within this series of compounds. Ld InMac is the intramacrophage assay carried out in THP-1 cells with *L. donovani* amastigotes.¹⁴ Number of biological replicates for all active compounds ≥ 2 ; PFI is the property forecast index;³¹ CLND is kinetic aqueous solubility measured using chemiluminescent nitrogen detection.²³

Table 5. In Vitro Profile of 30



Ld InMac (pEC ₅₀) ^a	6.3
THP-1 (pEC ₅₀) / HepG2 (pEC ₅₀) ^b	<4.3 / <4
Cl _i (mL·min ⁻¹ ·g ⁻¹) ^c	0.9 (mouse), 1.8 (human)
CLND solubility (μM) ^d	328
PFI ^e	4.9
Plasma Protein Binding (% unbound)	37%(Mouse), 33%(Human)

^aLd InMac is the intramacrophage assay carried out in THP-1 cells with *L. donovani* amastigotes.¹⁴ Data are the result of at least eight replicates. ^bHepG2 is a human liver cancer cell line. ^cCl_i is liver microsomal intrinsic clearance. ^dCLND is kinetic aqueous solubility measured using chemiluminescent nitrogen detection.²³ ^ePFI is the property forecast index.³¹

15 (Figure 3) against a panel of 210 human protein kinases at 5 μM (data not shown).

30 was selected for progression to the mouse in vivo efficacy model, and the greater solubility of **30** compared to **15** now allowed use of a vehicle that was suitable for subsequent toxicology studies (i.e., 0.5% HPMC, 0.4% Tween 80 and 0.5% benzyl alcohol) and investigation of higher doses within the model.

Analogue **30** demonstrated in vivo efficacy very close to our preclinical candidate target (i.e., >95% parasite suppression) at 100 mg/kg b.i.d. for 5 days, and a dose response study utilizing a 10 day regimen showed that a dose of 50 mg/kg b.i.d. achieved the same level of efficacy (Table 6).

Table 6. Mouse in Vivo Efficacy Profile of 30^a

oral regimen of 30	% suppression of parasite load compared to the control group	standard deviation (SD)
100 mg/kg b.i.d. for 5 days	94	5.24
10 mg/kg b.i.d. for 10 days	36	27.31
25 mg/kg b.i.d. for 10 days	74	4.49
50 mg/kg b.i.d. for 10 days	97	0.95

^aThe vehicle was 0.5% HPMC, 0.4% Tween 80 and 0.5% benzyl alcohol using 5 mice per dose level.

Table 7. PK Dose Escalation in Rats for 30

dose of 30 (mg/kg)	mean AUC _{0–last} h·ng/mL (%CV ^a)
10	162 (41)
100	2960 (33)
300	2383 (183)

^a%CV is the % of coefficient of variation. The vehicle was 1% methylcellulose in aqueous buffer using three rats per dose level.

A rat PK dose escalation study with **30** (Table 7) disappointingly showed greater than proportional increase in exposure between 10 and 100 mg/kg and then a saturation of absorption between 100 and 300 mg/kg limiting the maximum exposure that could be explored. This saturation of absorption at higher doses, together with high variability between animals, implied that solubility might still be problematic. Although **30** showed reasonable CLND solubility data (Table 5), the solubility profile in fasted state simulated intestinal fluid (FaSSIF)³² was poor (9 μg/mL). Other compounds within this series all showed a similar poor level of FaSSIF solubility (see **15**, **21**, and **30** in Table 8) except for **31**³³ (see Table 9 for structure), which had an improved profile (more discussion on **31** to follow). Care should always be taken when considering

Table 8. Profile of 15, 21, 30, and 31

	15	21	30	31
CLND solubility (μM) ^a	8	259	328	68
FaSSIF (μg/mL) ^b	<1	7	9	130
PFI ^c	7.2	5.0	4.9	8.0
pK _a ^d	3.2	3.7	nd	4.1
melting point (°C)	nd	273	218	135

^aCLND is kinetic aqueous solubility measured using chemiluminescent nitrogen detection.²³ ^bFaSSIF is fasted state simulated intestinal fluid solubility.³² ^cPFI is the property forecast index.³¹ ^dpK_a is the negative log₁₀ of acid dissociation constant.³⁵ nd is not determined.

FaSSIF solubility as variability between batches is known.³⁴ However, within this series of compounds, minimal FaSSIF variability was observed within the same batch and for **31** there was little variation between the lead optimization batches (see Table S20 in Supporting Information). Also, these compounds demonstrated that there was little correlation between FaSSIF and PFI or CLND within this series (see Table 8). Although different pH conditions were used to measure FaSSIF (pH 6.5) and PFI or CLND (pH 7.4), the measured pK_a values³⁵ of these compounds would suggest that the degree of protonation should have been similar under these different pH conditions.

Reviewing the general solubility equation (GSE, Yalkowsky and co-workers)³⁶ which relates lipophilicity and melting point to aqueous solubility (see eq 1), highlighted the importance of the melting point of the compound on its solubility.

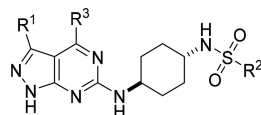
$$\log S = 0.5 - 0.01(\text{MP} - 25) - \log P \quad (1)$$

Equation 1: The general solubility equation (GSE), where *S* is solubility, *MP* is melting point in Celsius, and *P* is octanol–water partition coefficient. In practice, the GSE is commonly used where log *P* is replaced by log *D*_{pHx}, meaning log *S* is strictly log *S*_{pHx}.³⁷

Data in Table 8 indicates a reciprocal trend between melting point and FaSSIF solubility. To explore the potential means of modulating the high melting points, a small molecule crystal structure of **15** (Figure 6, as a representative example of the series) was obtained.

The crystal structure of **15** was shown to contain a single, fully ordered molecule in the centrosymmetric space group, *P*1̄. As can be seen in Figure 6, all three N–H groups act as hydrogen bond donors. Molecules of **15** form hydrogen-bonded dimers through reciprocal N20–H20···N19 interactions between inversion symmetry-related fused ring systems. These dimers are linked together by further hydrogen bonds between the sulfonamide and aminopyrimidine groups to form hydrogen-bonded columns within the structure. Additionally, the fused ring system and the pyridine in each molecule of **15** are

Table 9. In Vitro and FaSSIF Solubility Profiles of 1 and 31–40



Compound	R ¹	R ²	R ³	Ld InMac (pEC ₅₀) ^a	CLND (μM) ^b / FaSSIF (μg/mL) ^c	PFI ^d / melting point (°C)
31			OMe	6.4	68 / 130	8.0 / 135
32			OMe	5.9	311 / 53	5.8 / nd
33			OMe	6.7	258 / 16	5.8 / 217
34, single unknown enantiomer 1			OMe	5.4	412 / 283	4.9 / 81
35, single unknown enantiomer 2			OMe	5.2	421 / 208	4.9 / 79
36, single unknown enantiomer 1			H	5.6	≥ 310 / 88	5.4 / 219
37, single unknown enantiomer 2			H	5.7	≥ 292 / 118	5.4 / nd
1			H	5.9	99 / 64	5.5 / nd
38			H	5.3	52 / 23	5.5 / 263
39			OMe	6.6	≥ 382 / 50	6.1 / 127
40			OMe	6.0	≥ 365 / 87	6.1 / 125

^aLd InMac is the intramacrophage assay carried out in THP-1 cells with *L. donovani* amastigotes.¹⁴ Data are the result of at least three replicates. ^bCLND is kinetic aqueous solubility measured using chemiluminescent nitrogen detection.²³ ^cFaSSIF is fasted state simulated intestinal fluid solubility.³² ^dPFI is the property forecast index.³¹ nd is not determined.

approaching a coplanar arrangement [having a dihedral angle of 6.18(8)°], and this allows a π - π interaction between adjacent molecules within the columns. As such, **15** exhibited a highly stacked crystal lattice, therefore potentially explaining the low FaSSIF solubility. A number of analogues were therefore designed that would disrupt some of the hydrogen bonding seen in this crystal structure. From the past SAR, removal of N19

or N20-H (Figure 6) meant significant in vitro potency reduction (i.e., the N20-Me version of compound **15** demonstrated Ld InMac pEC₅₀ < 4.3 and THP pEC₅₀ < 4.3), so focusing on disruption of the other hydrogen bonds via introduction of strategically placed substituents was prioritized. A second strategy involved introducing substituents to reduce the overall planarity of this series, through either chiral centers or

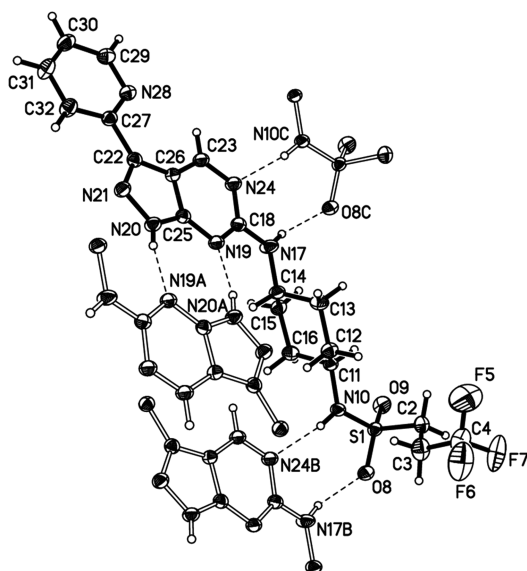


Figure 6. View of part of the crystal structure of **15**. The numbering scheme for the non-hydrogen atoms of the central molecule (depicted with the solid bond type) is shown in full. The hydrogen bonds associated with the central molecule are depicted as dashed lines. For clarity, only fragments containing the hydrogen bond donors and acceptors are shown for the surrounding molecules (with the open bond type). Anisotropic atomic displacement ellipsoids for the non-hydrogen atoms are shown at the 50% probability level. Hydrogen atoms are displayed with an arbitrarily small radius.

causing steric clashes. Indeed, some substituents could serve both of these desired functions and potentially improve the FaSSiF solubility (see Table 9).

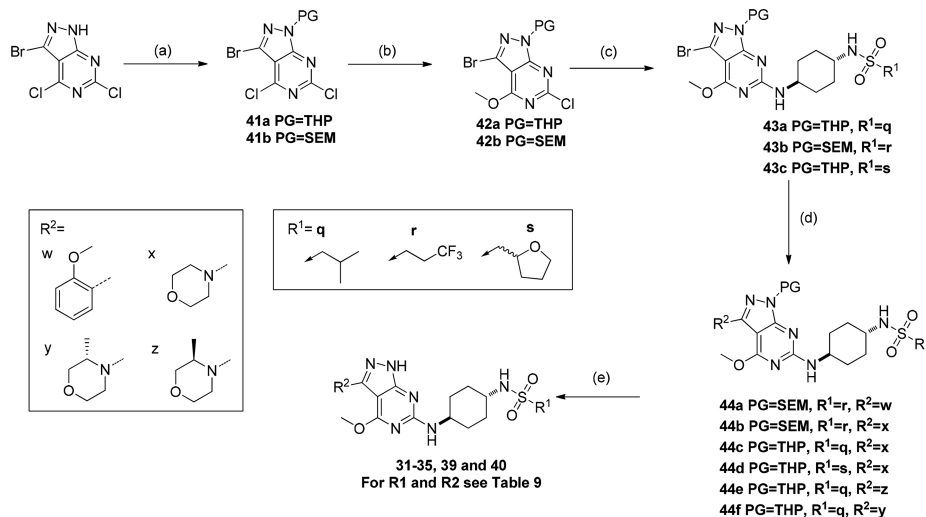
The 4-methoxy-1*H*-pyrazolo[3,4-*d*]pyrimidin-6-amino derivatives **31–35** were synthesized according to Scheme 5. Commercially available 3-bromo-4,6-dichloro-1*H*-pyrazolo[3,4-*d*]pyrimidine was THP-protected and the 4-chloro

selectively displaced with sodium methoxide to give **42a**. Treatment of **42a** with the appropriate amine **10a–c** in the presence of Hünig's base yielded **43a–c**. Suzuki coupling of **43a** with 2-methoxyphenylboronic acid or Buchwald–Hartwig coupling of **43b,c** with morpholine, followed by deprotection of the THP group, furnished compounds **31–35**. In the case of **44d**, THP deprotection was followed by separation of the enantiomers by chiral chromatography to give **34** and **35**. To generate the more challenging 3-methylmorpholine analogues **39** and **40**, a range of protecting groups, S_NAr conditions, and Buchwald–Hartwig coupling conditions were investigated. The conditions that gave the best results involved the use of SEM as the protecting group, which gave improved yields compared to THP. Subsequently, use of RuPhos as catalyst, tris(dibenzylideneacetone)dipalladium(0) as the palladium source, and potassium hexamethyldisilazide as base gave reasonable yields in the Buchwald–Hartwig coupling. Thus, treatment of **43d** with the appropriate enantiomer of 3-methylmorpholine under these conditions gave **44e–f**, with subsequent SEM deprotection yielding **39** and **40**.

As mentioned earlier, **31** (Tables 8 and 9) proved to be very interesting as it demonstrated that it was possible to identify compounds with improved FaSSiF solubility while maintaining intracellular potency. It was postulated that the additional methoxy group in the core could disrupt at least two or possibly four hydrogen bonds and/or force the phenyl ring to be out of the plane (Figure 6); in particular, it should disrupt the H-bonds formed by N17 and N24. As such, the addition of this OMe into the core of **21** (7 $\mu\text{g}/\text{mL}$) and **30** (9 $\mu\text{g}/\text{mL}$) was investigated in order to improve the FaSSiF solubility (see analogues **32** and **33** in Table 9). Pleasingly, both examples (**32** and **33**) demonstrated an increase in potency (in vitro), although only **32** showed an improvement in FaSSiF solubility compared to its corresponding parent compound (**21**).

Comparing **32** and **33** in more detail, it was postulated that variations to the sulphonamide could affect the distance between

Scheme 5. Synthesis of Compounds **31–35**, **39**, and **40**^a



^aReagents and conditions: (a) For THP, 3,4-dihydro-2*H*-pyran, *para*-toluenesulfonic acid monohydrate, THF, 70°C, 2 h, 79% (**41a**) or for SEM, 2-(trimethylsilyl)ethoxymethyl chloride, DIPEA, DCM, 0°C, 1.5 h, 100% (PG = THP, **42a**) or 98% (PG = SEM, **42b**); (b) NaOMe, MeOH, RT, 30 min, 100% (PG = THP, **42a**) or 98% (PG = SEM, **42b**); (c) **10a–c**, DIPEA, 1,4-dioxane, 110°C, 3 days, 40–51%; (d) 2-methoxyphenylboronic acid, Pd(PPh₃)₄, K₂CO₃, DMF, 130°C, 30 min for **44a** (87%) or morpholine, NaO^tBu, xantphos, Pd₂dba₃, dioxane, 110°C, overnight for **44b–d** 45–70%, or relevant 3-methylmorpholine, KHMDS, RuPhos, Pd₂dba₃, 1,4-dioxane, 110°C, 2 h for **44e,f** 47–50%; (e) HCl, MeOH, 60°C, 30 min to 1 h (THP deprotection of **44a–d**) or AcCl, MeOH, RT, 30 min to 1 h (SEM deprotection of **44e,f**) 32–83%.

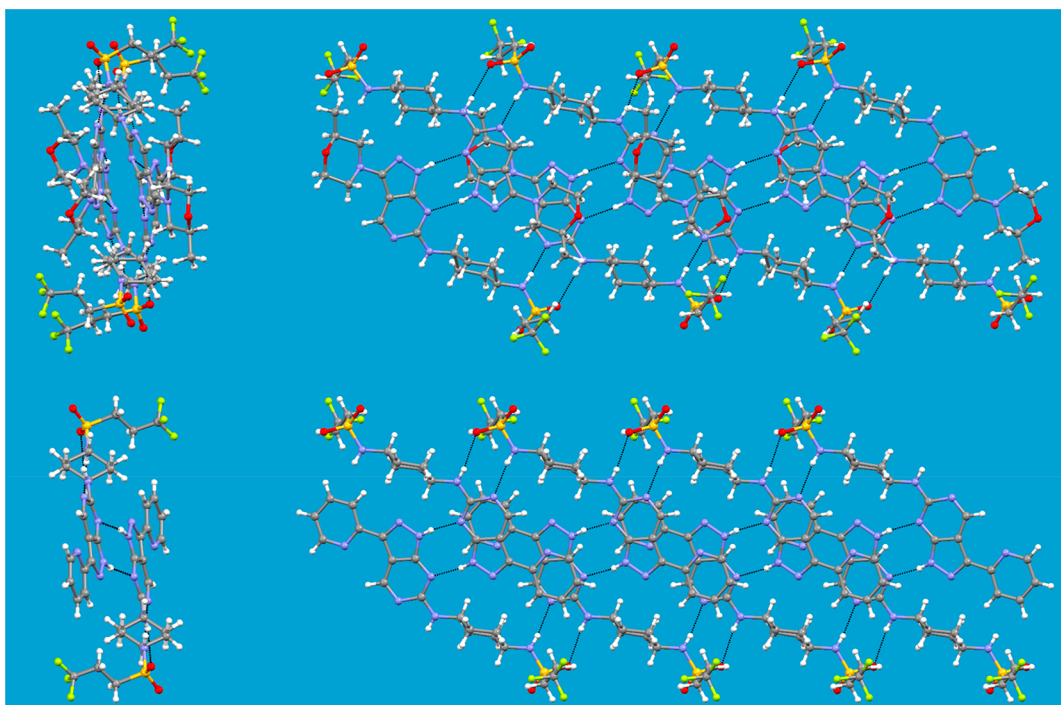


Figure 7. Hydrogen bonded columns in the crystal structures of **1** and **15**: (a) a view down a column in **1**; (b) an orthogonal view to (a); (c) a view down a column in **15**; (d) an orthogonal view to (c). Hydrogen bonds are displayed as black dotted lines.

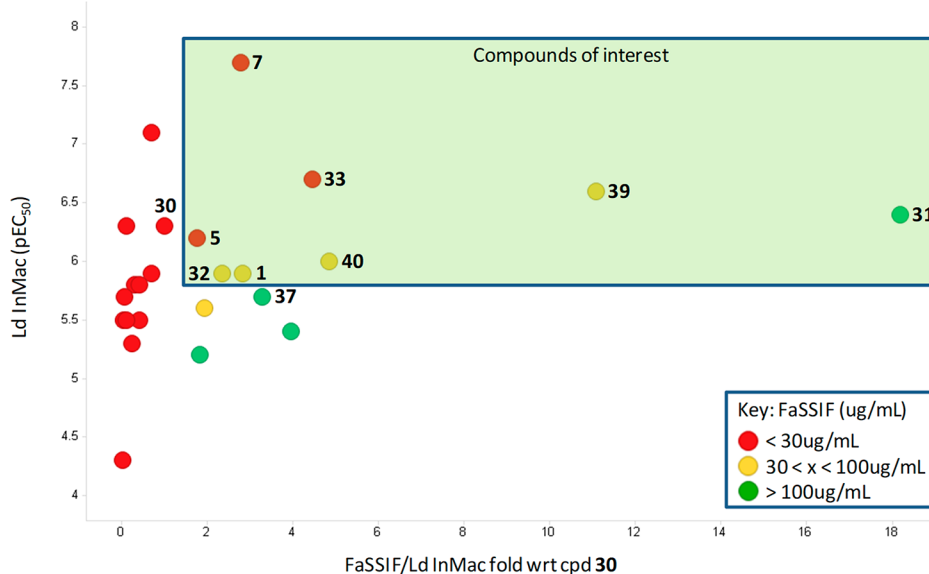


Figure 8. Ld InMac vs FaSSIF/Ld InMac fold wrt cpd **30**. Ld InMac is the intramacrophage assay carried out in THP-1 cells with *L. donovani* amastigotes.¹⁴ Data are the result of at least three replicates. FaSSIF/EC₅₀ fold wrt cpd **30** is the FaSSIF and Ld InMac ratio of a new compound compared to **30**.

the layers in the crystal structure and therefore influence the melting point. Thus, a bulkier sulphonamide, as exemplified by enantiomers **34** and **35**, were designed to further exploit this hypothesis (Table 9). Encouragingly, both enantiomers demonstrated an increase in FaSSIF solubility, albeit with a loss of intracellular potency compared to **32** and **33**.

Excited by this result, the alternative LHS that could break planarity and affect the stacking of the crystal structure were prioritized (i.e., **36**, **37**, **1**, and **38**). As Table 9 shows, all these compounds demonstrated increased FaSSIF solubility alongside similar or increased in vitro potency compared to **21**. It was

postulated that adding OMe to the core and *iso*-butyl sulphonamide to these examples could further increase in vitro potency while maintaining FaSSIF solubility, as had been seen for **33**. Indeed, both examples **39** and **40** showed a similar increase in potency (in vitro), although **39** had a lower FaSSIF solubility than expected compared to **40**. This observation between enantiomers was also mirrored for **1/38** and **36/37**, although the rationale for this is still unclear.

Interestingly, **1** crystallized in the noncentrosymmetric space group (*P1*) and has four independent molecules in the asymmetric unit (Figure 7). Although a different space group

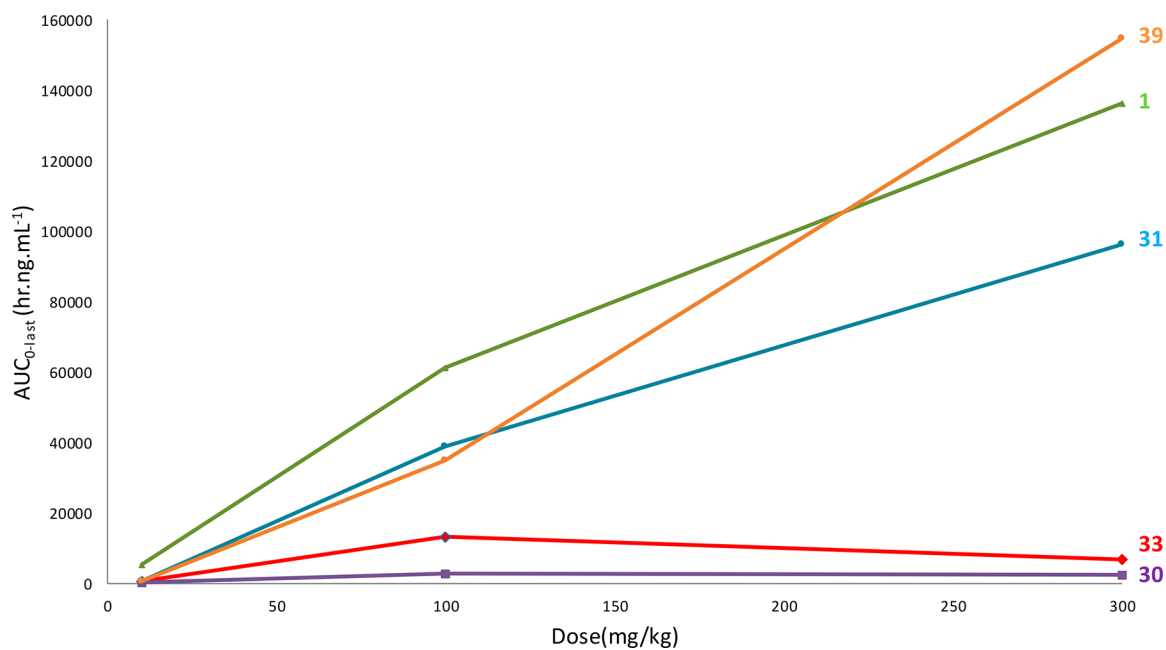


Figure 9. Rat PK dose escalation studies for 30, 31, 33, 1, and 39.

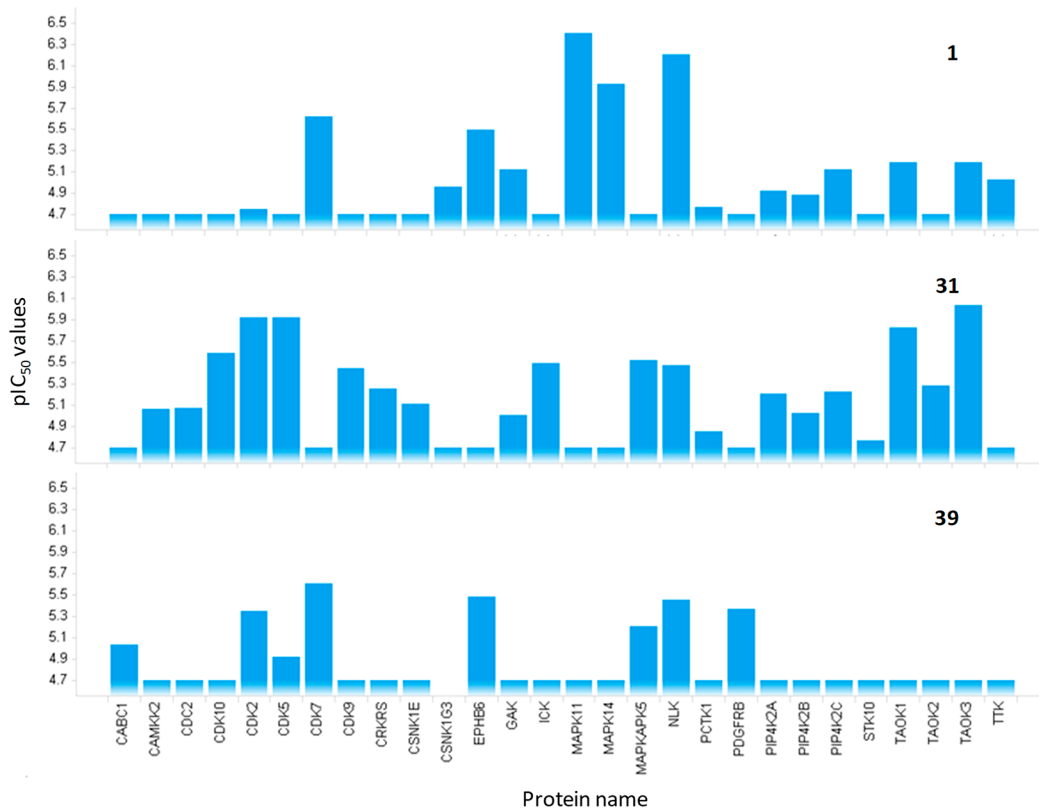


Figure 10. Human kinase selectivity profile of 1, 31, and 39. The figure shows all human protein kinases affected by any of the three compounds (no bar, protein was not identified; maximum compound concentration analyzed was $20 \mu\text{M}$).

to 15, analogous intermolecular hydrogen bonds were found to exist in 1 and 15, giving rise to columns in the same way. In cross-section, the columns are wider for 1 as they must accommodate the substituted morpholinyl groups and the removal of the π - π stacking. Although the structure of 1 has no centers of symmetry owing to the chiral ring, a pseudocentrosymmetric arrangement has been adopted. In effect, the four

independent molecules in 1 increase the flexibility of the system, allowing the same hydrogen bonds to exist as in 15 despite the much bulkier, chiral ring being present. Overall, however, the packing in 1 is clearly less efficient than 15, leading to a density of 1.405 g cm^{-3} (versus 1.511 g cm^{-3}) at the temperature of the experiments (150 K) and a packing coefficient of 0.676 (versus 0.699). In this respect, the deliberate attempt to disrupt the

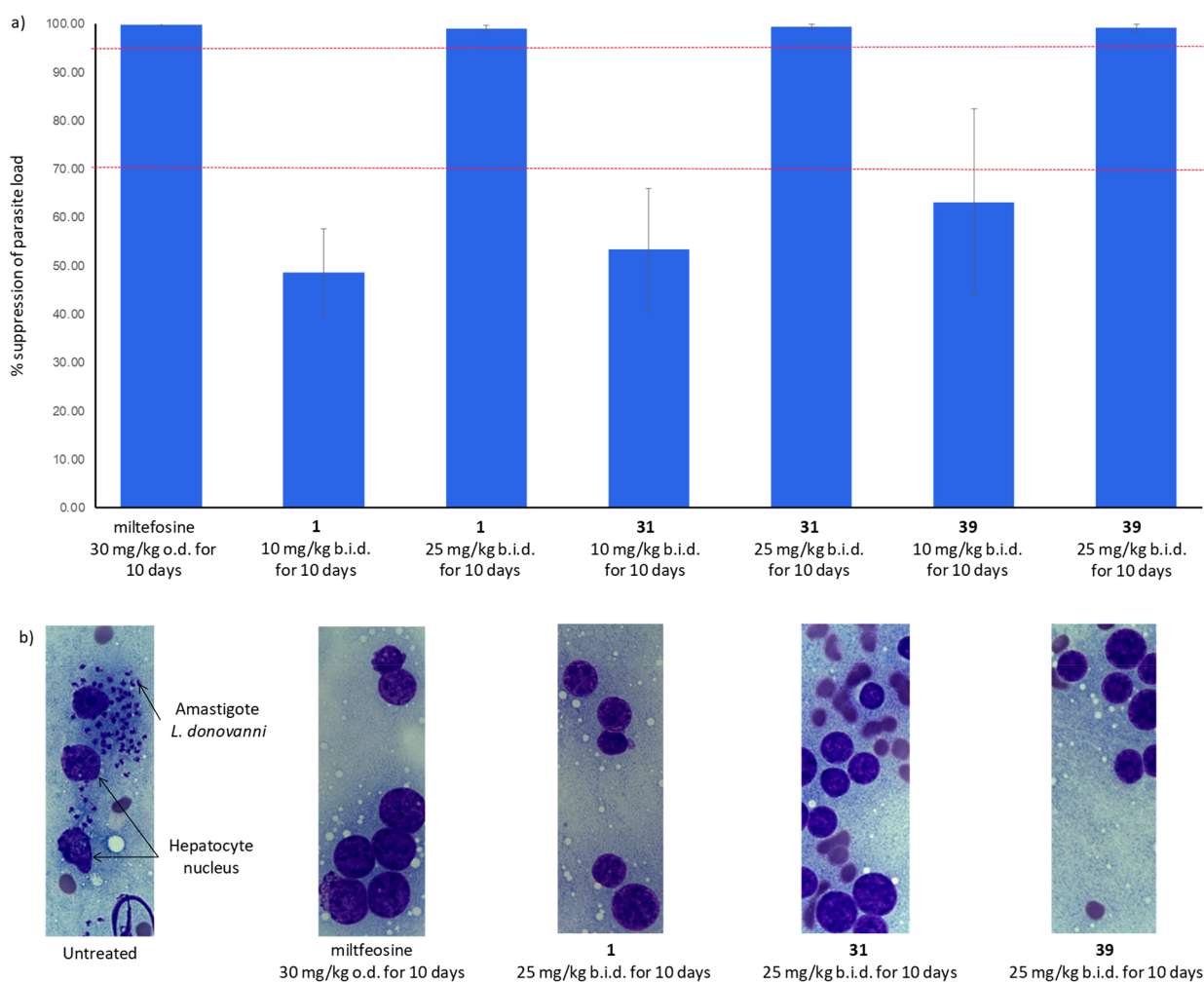


Figure 11. (a) In vivo efficacy of **31**, **1**, and **39** compared to miltefosine; (b) mouse liver smears from in vivo efficacy model for untreated, miltefosine, **31**, **1**, and **39**. The mean LDU values from individual animal livers were compared to the control to give the percentage (%) suppression of parasite load in Balb/c mice (that were infected with *L. donovani*). Vehicle used for **31**, **1**, and **39** was 0.5% HPMC, 0.4% Tween 80, and 0.5% benzyl alcohol, and deionized water for miltefosine. This experiment was carried out using five mice per dose level. Error bars represent the standard deviation (SD). Lead optimization criteria was 70% suppression in liver parasite burden, while the preclinical candidate was >95%.

packing found in **15** was a success and helped to improve FaSSIF solubility while maintaining in vitro potency (Table 8 and 9).

Upon analyzing the data shown in Table 9, it became clear that there was no correlation between FaSSIF solubility and in vitro potency. Consequently, multiparameter optimization was pursued (eq 2), whereby the FaSSIF and Ld InMac ratio of a new compound was compared to a reference compound (i.e. **30**), coupled with a potency filter of Ld InMac pEC₅₀ ≥ 5.8, and this allowed more informed compound progression decisions.

FaSSIF/Ld InMac fold wrt cpd 30

$$= \text{FaSSIF} \left(\frac{\text{new cpd}}{\text{cpd 30}} \right) \times \text{Ld InMac EC}_{50} \left(\frac{\text{cpd 30}}{\text{new cpd}} \right) \quad (2)$$

Equation 2: FaSSIF/Ld InMac fold wrt cpd 30.

The reasoning behind the additional in vitro potency filter was that compounds from this series with Ld InMac pEC₅₀ < 5.8 were never seen to demonstrate desirable in vivo efficacy at a further reduced dose (i.e., ≤25 mg/kg b.i.d.), even when having progressable FaSSIF solubility (for example, compound **37** demonstrated 65% parasite suppression at 25 mg/kg b.i.d. for 10 days).

Figure 8 highlights the compounds of interest based on the selection criteria discussed above (i.e. **31**, **33**, **1**, and **39**), which were subsequently progressed to rat PK dose escalation studies (Figure 9). Compounds **5** and **7** were rejected due to metabolic instability when incubated with mouse liver microsomes (Table 2), whereas **32** and **40** showed no advantage in terms of “FaSSIF/Ld InMac fold wrt cpd 30” profile over their counterparts **33** and **39**, respectively (Table 9).

33 was progressed into rat PK on the basis of high potency compensating for low FaSSIF solubility. However, it gave very similar exposures to **30** upon dose escalation (Figure 9), demonstrating that it was not suitable for further progression. Pleasingly, however, 3 out of the 4 compounds (**31**, **1**, and **39**) demonstrated notably superior exposure to **30** as measured by the AUC (Figure 9), in line with the multiparameter hypothesis. Furthermore, these compounds all showed a dose proportional exposure increase, which would be important in further development of the compound series, particularly when determining potential therapeutic indices.

Chemoproteomic profiling on Kinobeads was performed in a mixed human cell/tissue extract, to identify potential human off-targets for **31**, **1**, and **39** (Figure 10). The compounds were

tested for their activity against >260 human protein kinases, and IC₅₀ values were generated. Figure 10 shows only kinases affected by any of the three compounds, indicating that the three compounds had different human kinase profiles. Cdk4 was only identified in the experiment for 39 (IC₅₀ > 20 μM). Additionally, 31 and 39 did show potency against Cdk2, albeit 9- or 35-fold less potent respectively than the closest analogue from Ding and co-workers,¹⁹ where it was unaffected by 1. However, the extent of inhibition of these human kinases was not sufficient to preclude progression for any one compound. Interestingly, performing similar dose–response experiments using leishmania parasite lysate for 8 identified CRK12 (IC₅₀ 3 nM), MPK9 (IC₅₀ 105–181 nM), and CRK6 (IC₅₀ 194–363 nM).¹⁷

On this basis, 31, 1, and 39 were progressed into in vivo efficacy studies, where all three gave sufficient parasite suppression to be considered as preclinical development candidates at 25 mg/kg b.i.d. for 10 days (Figure 11). As such, all three compounds were profiled in key in vitro and ex vivo safety assays (Table 10) in order to select a lead compound to prioritize for a 7 day toxicology study.

Table 10. Comparison of three Key Compounds (31, 1, and 39)

	31	1	39
Ld InMac (pEC ₅₀) ^a	6.4	5.9	6.6
Cl _i (mL·min ⁻¹ ·g ⁻¹) ^b	1.1 (mouse)	<0.5 (mouse), 0.7 (human)	0.6 (mouse), 2.5 (human)
mouse in vivo efficacy (>95% parasite suppression)	25 mg/kg b.i.d. @ 10 d	25 mg/kg b.i.d. @ 10 d	25 mg/kg b.i.d. @ 10 d
PFI ^c	8.0	5.5	6.1
FaSSIF (μg/mL) ^d	25	17 ^e	33
CYP3A4 (pIC ₅₀)	5.2	<4.4	<4.4
Ames ³⁸	–ve @ 1500 μg/plate	–ve @ 1500 μg/plate	–ve @ 1500 μg/plate
MLA ^f	–ve @ 5 μg/mL	–ve @ 120 μg/mL	equivocal @ 350 μg/mL
hERG (IC ₅₀ , μM) ^{39,40}	17.5	>30	>30
RVW ^g	QT shortening (11.3% @ 10 μM)	QT shortening (8.9% @ 30 μM)	QT shortening (15.2% @ 100 μM)

^aLd InMac is the intramacrophage assay carried out in THP-1 cells with *L. donovani* amastigotes.¹⁴ Data are the result of at least six replicates. ^bCl_i is liver microsomal intrinsic clearance. ^cPFI is the property forecast index;³¹ –ve is negative. ^dFaSSIF is fasted state simulated intestinal fluid solubility.³² ^eMelting point for this batch was 262 °C. ^fMLA is mouse lymphoma assay.⁴¹ ^gRVW is rabbit ventricular wedge.⁴²

Following a form screen, the most stable form was identified and the corresponding FaSSIF solubility is reported in Table 10. Apparent inhibition by 31 in an in vitro hERG assay^{39,40} prompted progression of all three compounds to the ex vivo rabbit ventricular wedge (RVW) assay.⁴² Interestingly, they all showed a similar effect of QT shortening, which appears to be independent of hERG in vitro potency. The clinical relevance of this QT shortening finding and its translation in vivo was unclear.⁴³ There were no changes to the remaining QT parameters tested, and the risk of QT prolongation and Torsade de pointes (TdP) arrhythmia in humans was assessed as low based on these results. Because there were only minor differences, all three compounds were progressed into 7 day rat toxicology and rat cardiovascular studies (Table 11).

Table 11. Summary of 7 Day Rat Toxicology and Rat Cardiovascular Data for 31, 1, and 39

	31	1	39
7 day rat toxicology doses tolerated doses	100, 300, and 1000 mg/kg	100, 300, and 1000 mg/kg	100, 300, and 1000 mg/kg
therapeutic index (TI) ^h	100 and 300 mg/kg TI@300 mg/kg is 19-fold	100, 300, and 1000 mg/kg TI@300 mg/kg is 13-fold	100 and 300 mg/kg TI@300 mg/kg is 1.8-fold
In life and clinical signs ⁱ	1000 mg/kg; terminated day 7, ↓food consumption and piloerection, irregular breathing (+ others)	Day 7 exposure saturated 1000 mg/kg ≡ 300 mg/kg/day none	1000 mg/kg; terminated day 6, body weight reduction in all animals, 50% reduction in food consumption, one animal stomach erosion/ulceration
macro observations	stomach distension	none	nd
histopathology	1000 mg/kg: Multiple organ changes 300 mg/kg: pancreas and kidney vacuolation	1000 mg/kg: (2/4), minimal adrenal vacuolar degeneration	nd
clinical pathology ^j	300 mg/kg - (2/4) ↑ cTnl ^k and NT-proANP, ↑ total bilirubin, cholesterol, phosphorus, and monocytes, ↓ albumin and triglycerides	1000 mg/kg to ↑ ALP, ^c ↓ calcium and ↑ plasma glucose 300 and 1000 mg/kg to ↓ RBC, ^d HCT, ^e Hb, ^f ↓ Total protein and albumin 300 mg/kg to ↑ triglycerides	nd
liver gene expression profiling ^g	all panels were NEGATIVE CYP1A1 gene ↑ increase all doses max 43X	all panels were NEGATIVE CYP1A1 gene, no increase	nd
rat cardiovascular study ^k	no significant effect up to 600 mg/kg (TI = 12-fold)	no significant effect up to 1000 mg/kg (TI = 3-fold)	nd

^acTnl is cardiac troponin I. ^bNT-proANP is N-terminal proatrial natriuretic peptide. ^cALP is alkaline phosphatase. ^dRBC is red blood cells. ^eHCT is hematocrit. ^fHb is hemoglobin. ^gLiver gene expression profiling is a GSK panel of genes reflecting mechanisms of hepatic toxicity; nd not determined. ^hTI = AUC_{0–24} day 7 of rat toxicology study/AUC_{0–24} day 10 of mouse efficacy model. ⁱ↑ means increase and ↓ is decrease. ^j↑ means increase and ↓ is decrease over controls. ^kTI = free C_{max} day 1 of rat cardiovascular study/free C_{max} day 1 of mouse efficacy model.

The outcome of the 7 day studies was the deselection of **39**, as the therapeutic index (TI) was not sufficient for progression (Table 11). **1** was selected as the preclinical candidate for VL (as opposed to **31**) due to the fact the TI was limited by exposure and not by an adverse event, coupled with no direct inhibition of CYP3A4 and no flags within liver gene expression profiling panel (which can lead to problematic drug–drug interactions that are particularly relevant due to the frequency of VL/HIV coinfections).⁴⁴

SUMMARY AND CONCLUSION

Initial hit **4** demonstrated a promising profile (Table 1) but highlighted the need to optimize in vitro potency and mouse metabolic stability in order to test this series within an in vivo VL animal study. With those properties improved and selectivity against a panel of human kinases, **15** was progressed to such an in vivo model, where it demonstrated an 85% suppression in parasite load within the liver (Figure 4). However, due to low CLND solubility, **15** was not progressed further because it required the use of a vehicle that was not acceptable in downstream toxicological studies. Successfully using PFI to improve solubility of this series led to compound **30**, which demonstrated candidate quality efficacy using a formulation that could be used for toxicological studies (Table 6). Dose escalation in rats demonstrated that **30** exhibited variable nonlinear exposure, limiting the ability to assess its therapeutic index in toxicological studies (Table 7). It was speculated that the low FaSSIF solubility was driving this variable nonlinear exposure. After investigating the small molecule crystal structure of **15** (Figure 6), disrupting certain hydrogen bonds and breaking planarity by introducing specific substituents became the primary medicinal chemistry focus. Multiple compounds demonstrated improved FaSSIF solubility, however, the use of a mathematical comparison to **30** and a potency filter (eq 2 and Figure 8) aided the selection of **31**, **33**, **1**, and **39**. All except **33** (where high potency compensated for low FaSSIF solubility) demonstrated superior exposure compared to **30** (Figure 9). This demonstrated that FaSSIF solubility gave a better correlation to rat PK exposure than CLND for this series, likely due to being more relevant to biological systems and the fact that it is a thermodynamic measurement of solubility. To further differentiate between **31**, **1**, and **39** (Table 10), all were progressed into 7 day rat toxicological studies (Table 11). **1** was finally selected as a preclinical candidate for VL, and definitive safety studies are being conducted to support clinical progression. Compound **1** is one of only a handful of compounds worldwide that have reached preclinical candidate status for VL, highlighting the need and also the achievement.

EXPERIMENTAL SECTION

General Experimental Information. Chemicals and solvents were purchased from the Aldrich Chemical Co., Fluka, Fluorochem, ABCR, VWR, Acros, Fisher Chemicals, and Alfa Aesar and were used as received unless otherwise stated. Air- and moisture-sensitive reactions were carried out under an inert atmosphere of argon in oven-dried glassware. Analytical thin-layer chromatography (TLC) was performed on precoated TLC plates (layer 0.20 mm silica gel 60 with fluorescent indicator UV254, from Merck). Developed plates were air-dried and analyzed under a UV lamp (UV254/365 nm). Flash column chromatography was performed using prepacked silica gel cartridges (230–400 mesh, 40–63 μ m, from SiliCycle) using a Teledyne ISCO Combiflash Companion, or Combiflash Retrieve. ¹H NMR, ¹³C NMR, ¹⁹F NMR, and 2D-NMR spectra were recorded on a Bruker Avance DPX 500 spectrometer (¹H at 500.1 MHz, ¹³C at 125.8 MHz, ¹⁹F at

470.5 MHz). Chemical shifts (δ) are expressed in ppm recorded using the residual solvent as the internal reference in all cases. Signal splitting patterns are described as singlet (s), doublet (d), triplet (t), quartet (q), multiplet (m), broad (b), or a combination thereof. Coupling constants (J) are quoted to the nearest 0.1 Hz. LC-MS analyses were performed with either an Agilent HPLC 1100 series connected to a Bruker Daltonics MicrOTOF or an Agilent Technologies 1200 series HPLC connected to an Agilent Technologies 6130 quadrupole LC/MS, where both instruments were connected to an Agilent diode array detector. Mobile phase was water/acetonitrile + 0.1% HCOOH, or water/acetonitrile + 0.1% NH₃; linear gradient 80:20 to 5:95 over 3.5 min, and then held for 1.5 min; flow rate 0.5 mL min⁻¹. All intermediates had a measured purity of >90% as determined using this analytical LC-MS system unless otherwise noted. All assay compounds had a measured purity of \geq 95% as determined using this analytical LC-MS system (TIC and UV). High resolution electrospray measurements were performed on a Bruker Daltonics MicrOTOF mass spectrometer. Microwave-assisted chemistry was performed using a Biotage Initiator microwave synthesizer.

3,3,3-Trifluoro-N-(trans-4-((3-((S)-2-methylmorpholino)-1H-pyrazolo[3,4-d]pyrimidin-6-yl)amino)cyclohexyl)propane-1-sulfonamide 1. 29a (91 g, 173 mmol) was dissolved in dioxane (1.2 L), then hydrazine hydrate 85% (173.2 g, 3.5 mol) was added and the reaction stirred at 90 °C for 18 h. The mixture was cooled to 25 °C, where H₂O (800 mL) and EtOAc (800 mL) was added and the mixture was stirred at room temperature for 20 min. The organic phase was separated, and the aqueous phase was extracted with EtOAc (3 \times 1.5 L). The combined organic phases were washed with brine (2 \times 2 L) and dried over Na₂SO₄. The solvent was removed under vacuum, and EtOAc (400 mL) was added to the residue and stirred at room temperature for 1 h. The resulting mixture was filtered, the cake was washed with EtOAc (100 mL), and the filtrate was dried in vacuo to afford a crude solid. This solid was then purified by recrystallization from methanol (400 mL) to give **1** (40 g, 81 mmol, 47% yield) as a light-green solid. ¹H NMR (DMSO-*d*₆): δ 11.93 (s, 1H), 8.82 (s, 1H), 7.33 (d, J = 7.6 Hz, 1H), 7.14 (s, 1H), 3.86 (dd, J = 10.9 and 2.9 Hz, 1H), 3.73–3.55 (m, 5H), 3.31–3.09 (m, 3H), 2.90–2.81 (m, 1H), 2.66–2.50 (m, 3H), 1.92 (br s, 4H), 1.39–1.29 (m, 4H), 1.15 (d, J = 6.2 Hz, 3H). ¹³C NMR (DMSO-*d*₆): δ 160.5, 157.3, 154.0, 151.3, 127.9 (q, J_{CF} = 128 Hz), 71.3, 65.9, 54.6, 52.0, 49.9, 47.9, 45.4, 33.1 (2C), 31.2 (2C), 28.9 (q, J_{CF} = 29.9 Hz), 19.2. ¹⁹F NMR (DMSO-*d*₆) δ –64.4. HRMS (ES⁺): m/z [M + H]⁺ calcd for C₁₉H₂₉N₇O₃F₃S 492.1999, found 492.1998. Enantiopurity determined using a chiral column: Chiralpak AD-3, 3 mm, 0.46 cm \times 10 cm, acetonitrile/MeOH = 50/50 + 0.2% isopropyl amine, 30 mL/min, 298 K, 254 nm. First enantiomer (compound **38**, minor) R_t = 6.6 min, second enantiomer (**1**, major) R_t = 9.7 min. *ee* measured: 99.2%.

N-Cyclohexyl-3-isobutyl-1H-pyrazolo[3,4-d]pyrimidin-6-amine 3. A mixture of **11a** (100 mg, 0.44 mmol) and cyclohexylamine (48 mg, 0.48 mmol) in *n*-butanol (4 mL) was stirred at 100 °C for 15 min then cooled to room temperature. Hydrazine hydrate (360 μ L, 1.76 mmol) was added and the mixture stirred in a sealed tube at 150 °C for 45 min (microwave). The solution was cooled, solvent evaporated, and the crude mixture chromatographed (0–10% methanol/DCM) to give **3** (64 mg, 0.23 mmol, 53% yield). ¹H NMR (DMSO-*d*₆): δ 12.57 (s, 1H), 8.74 (s, 1H), 7.12 (bs, 1H), 3.72 (bs, 1H), 2.64 (d, J = 7.2 Hz, 2H), 2.05 (sept, J = 6.9 Hz, 1H), 1.93–1.89 (m, 2H), 1.77–1.71 (m, 2H), 1.64–1.58 (m, 1H), 1.35–1.13 (m, 5H), 0.91 (d, J = 6.6 Hz, 6H). ¹³C NMR (DMSO-*d*₆): δ 160.6, 157.5, 153.6, 145.7, 106.7, 49.6, 36.5, 32.7, 28.6 (2C), 25.9 (2C), 25.4 (2C), 22.9. HRMS (ES⁺): m/z [M + H]⁺ calcd for C₁₅H₂₄N₅ 274.2032, found 274.2018.

N-(trans-4-((3-Isobutyl-1H-pyrazolo[3,4-d]pyrimidin-6-yl)amino)cyclohexyl)-2-methylpropane-1-sulfonamide 6. **6** was obtained by an analogous method to **3** (28 mg, 0.07 mmol, 44% yield). ¹H NMR (DMSO-*d*₆): δ 12.50 (bs, 1H), 8.65 (s, 1H), 7.14 (s, 1H), 6.94 (d, J = 7.6 Hz, 1H), 3.03–2.88 (m, 2H), 2.81 (d, J = 6.3 Hz, 2H), 2.55 (d, J = 7.1 Hz, 2H), 2.03–1.91 (m, 2H), 1.87–1.79 (m, 4H), 1.27–1.21 (m, 4H), 0.93 (d, J = 6.8 Hz, 6H), 0.81 (d, J = 6.6 Hz, 6H). HRMS (ES⁺): m/z [M + H]⁺ calcd for C₁₉H₃₃N₆O₂S 409.2386, found 409.2400.

3,3,3-Trifluoro-N-(trans-4-((3-isobutyl-1H-pyrazolo[3,4-d]pyrimidin-6-yl)amino)cyclohexyl)propane-1-sulfonamide 7. **7** was obtained by an analogous method to **3** (18 mg, 0.04 mmol, 25% yield). ¹H NMR (DMSO-*d*₆): δ 12.67 (s, 1H), 8.82 (s, 1H), 7.37 (d, *J* = 7.6 Hz, 1H), 7.25 (s, 1H), 3.63 (s, 1H), 3.32–3.27 (m, 2H), 3.16 (s, 1H), 2.68–2.61 (m, 4H), 2.08–2.00 (m, 1H), 2.08–2.00 (m, 4H), 1.38–1.28 (m, 4H), 0.91 (d, *J* = 6.5 Hz, 6H). HRMS (ES⁺): *m/z* [M + H]⁺ calcd for C₁₈H₂₈F₃N₆O₂S 449.1947, found 449.1952.

N-(trans-4-((3-(2-Methoxyphenyl)-1H-pyrazolo[3,4-d]pyrimidin-6-yl)amino)cyclohexyl)-2-methylpropane-1-sulfonamide 8. **8** was obtained by an analogous method to **3** (270 mg, 0.59 mmol, 72% yield). ¹H NMR (DMSO-*d*₆): δ 13.08 (s, 1H), 8.76 (s, 1H), 7.66 (dd, *J* = 1.7, 7.6 Hz, 1H), 7.47–7.42 (m, 1H), 7.27–7.17 (m, 2H), 7.09–7.00 (m, 2H), 3.87 (s, 3H), 3.75–3.65 (m, 1H), 3.15–3.08 (m, 1H), 2.91 (d, *J* = 6.6 Hz, 2H), 2.17–2.07 (m, 1H), 2.02–1.91 (m, 4H), 1.44–1.35 (m, 4H), 1.04 (d, *J* = 6.6 Hz, 6H). ¹³C NMR (DMSO-*d*₆): 160.5, 157.6, 155.7, 142.3, 130.5, 130.3, 122.1, 121.1, 112.1, 60.4, 55.8, 51.9, 49.1, 33.3 (2C), 31.2 (2C), 25.0, 22.8 (2C). HRMS (ES⁺): *m/z* [M + H]⁺ calcd for C₂₂H₃₁N₆O₃S 459.2178, found 459.2183.

2-Methyl-N-(trans-4-((3-(pyridin-2-yl)-1H-pyrazolo[3,4-d]pyrimidin-6-yl)amino)cyclohexyl)propane-1-sulfonamide 9. **9** was obtained by an analogous method to **3** (630 mg, 1.5 mmol, 59% yield). ¹H NMR (DMSO-*d*₆): δ 13.32 (bs, 1H), 9.34 (s, 1H), 8.71 (d, *J* = 4.2 Hz, 1H), 8.08 (d, *J* = 8.0 Hz, 1H), 7.93–7.89 (m, 1H), 7.45 (bs, 1H), 7.49–7.39 (m, 1H), 7.04 (d, *J* = 6.0 Hz, 1H), 3.81–3.61 (m, 1H), 3.12–3.06 (m, 1H), 2.92 (d, *J* = 6.4 Hz, 2H), 2.13–2.05 (m, 1H), 1.97–1.94 (m, 4H), 1.41–1.31 (m, 4H), 1.04 (d, *J* = 6.7 Hz, 6H). ¹³C NMR (DMSO-*d*₆): δ 160.8, 158.2, 156.0, 159.9, 152.7, 150.0, 144.3, 137.4, 123.7, 120.1, 60.5, 51.9, 49.1, 33.3 (2C), 31.2 (2C), 25.0, 22.8. HRMS (ES⁺): *m/z* [M + H]⁺ calcd for C₂₀H₂₈N₇O₂S 430.2020, found 430.2024.

N-(trans-4-Aminocyclohexyl)-2-methylpropane-1-sulfonamide 10a. To a solution of *tert*-butyl *N*-(4-aminocyclohexyl)carbamate (24 g, 112 mmol) in THF (800 mL) at –78 °C was added *n*-butyl lithium (2.5 M in hexanes, 49.3 mL, 123 mmol) dropwise and stirred for 20 min at –78 °C. The solution was warmed to –20 °C and stirred for 15 min, then cooled to –78 °C. 3,3,3-Trifluoropropane-1-sulfonyl chloride (15.4 mL, 118 mmol) was added dropwise, stirred for a further 5 min at –78 °C, and then warmed to room temperature where it was stirred for 1 h. The reaction mixture was quenched with 1 M HCl (50 mL) and EtOAc (500 mL), and the aqueous layer separated and extracted with EtOAc (2 × 500 mL). The combined organic layers were dried with Na₂SO₄ and filtered, and the remaining solvent was evaporated to give a white solid (33.5 g). This crude material (33.5 g) was dissolved in DCM (400 mL), and TFA (38.3 mL) added at room temperature and stirred overnight. The solvent was removed under vacuum to give an oil, and Et₂O (70 mL) was added to precipitate **10a** as a white solid (35 g, 100 mmol, 89% yield over two steps). ¹H NMR (DMSO-*d*₆): δ 7.97 (br s, 2H), 7.15 (d, *J* = 7.3 Hz, 1H), 3.02–2.96 (m, 1H), 2.86 (d, *J* = 6.5 Hz, 2H), 2.46 (ddd, *J* = 3.7, 7.2, 14.5 Hz, 1H), 2.09–2.02 (m, 1H), 1.81 (t, *J* = 5.4 Hz, 2H), 1.75–1.69 (m, 2H), 1.27–1.16 (m, 2H), 1.11–1.03 (m, 2H), 1.00 (d, *J* = 6.8 Hz, 6H).

N-(trans-4-Aminocyclohexyl)-3,3,3-trifluoropropane-1-sulfonamide 10b. This reaction was performed in two batches. To a suspension of *tert*-butyl ((1,4-*trans*)-4-aminocyclohexyl)carbamate (30 g, 140 mmol) in THF (1.33 L), cooled at –78 °C, *n*-butyl lithium (56 mL, 140 mmol) was added dropwise. The resulting mixture was stirred at –78 °C for 20 min and at –10 °C for 10 min. After cooling to –78 °C, 3,3,3-trifluoropropane-1-sulfonyl chloride (17.64 mL, 140 mmol) was added. After stirring for 1.5 h, it was allowed to warm to RT and stirred for 20 min. The reaction mixture was diluted with H₂O (500 mL), followed by addition of 2 M HCl (20 mL) and was extracted with EtOAc (400 mL). The organic layer was dried over Na₂SO₄, filtered, and concentrated to give *tert*-butyl ((1,4-*trans*)-4-(3,3,3-trifluoropropylsulfonamido)cyclohexyl)carbamate as a white solid (43.5 g, 116 mmol, 83% yield). ¹H NMR (DMSO-*d*₆): δ 7.33 (d, *J* = 6.4 Hz, 1H), 6.77–6.70 (d, *J* = 6.7 Hz, 1H), 3.30–3.23 (m, 2H), 3.17–3.01 (m, 2H), 2.70–2.56 (m, 2H), 1.87–1.67 (m, 4H), 1.36 (s, 9H), 1.31–1.13 (m, 4H). TFA (182 mL, 2377 mmol) was added to a solution of *tert*-butyl ((1,4-*trans*)-4-(3,3,3-trifluoropropylsulfon-

amido)cyclohexyl)carbamate (89 g, 238 mmol) in DCM (732 mL), cooled to 0 °C. The reaction mixture was stirred at RT overnight. The mixture was concentrated to dryness and coevaporated with Et₂O (100 mL) to give **10b** as a white solid (93.5 g, 238 mmol, quant yield). ¹H NMR (DMSO-*d*₆): δ 7.89 (br s, 2H), 7.43 (d, *J* = 7.5 Hz, 1H), 3.34–3.24 (m, 2H), 3.16–3.05 (m, 1H), 2.99–2.86 (m, 1H), 2.72–2.56 (m, 2H), 1.95–1.84 (m, 4H), 1.43–1.21 (m, 4H).

1-(2-Chloro-4-methoxyppyrimidin-5-yl)-3-methylbutan-1-one 11a. To a solution of 5-bromo-2-chloro-4-methoxyppyrimidine (1.11 g, 5 mmol) in THF (20 mL) at –40 °C was added a solution of *iso*-propyl magnesium chloride (3 mL, 6.5 mmol, 2 M in ether) dropwise over 10 min and the resulting suspension stirred for 15 min. A solution of *iso*-valeraldehyde (700 μL, 6.5 mmol) in THF (2 mL) was added dropwise over 10 min, stirring continued for 30 min and the reaction quenched with methanol (1 mL), allowed to warm to room temperature, and the solvent evaporated. Crude material was taken up in DCM (20 mL), washed with 2 M HCl (20 mL), dried, and evaporated. Crude material was dissolved in DCM (20 mL), Dess–Martin periodinane (2.97 g, 7 mmol) added, and the reaction mixture stirred for 1 h. A mixture of satd sodium bicarbonate (20 mL)/satd sodium thiosulfate (20 mL) was added and stirring continued for 30 min. The organic layer was separated, dried, evaporated, and crude material chromatographed (0–40% EtOAc/heptane) to yield **11a** (0.65 g, 2.9 mmol, 57% yield over 2 steps). ¹H NMR (DMSO-*d*₆): δ 8.84 (s, 1H), 4.24 (s, 3H), 2.90 (d, *J* = 6.8 Hz, 2H), 2.34–2.27 (m, 1H), 1.06 (d, *J* = 6.6 Hz, 6H). MS (ES⁺) *m/z* 229.1, 231.1 [M + H]⁺.

3,3,3-Trifluoro-N-(trans-4-((3-(pyridin-2-yl)-1H-pyrazolo[3,4-d]pyrimidin-6-yl)amino)cyclohexyl)propane-1-sulfonamide 15. **11c** (1.25 g, 5 mmol), **10b** (1.50 g, 5.5 mmol), and DIPEA (1.05 mL, 6 mmol) in ethanol (20 mL) were stirred at 120 °C for 30 min (microwave). After cooling to room temperature, hydrazine hydrate (1.1 mL, 20 mmol) was added and the mixture stirred at 150 °C for 30 min (microwave). Upon cooling, a precipitate formed, which was collected, washed with ethanol, and dried in vacuo to give **15** (1.67 g, 3.6 mmol, 71% yield). ¹H NMR (DMSO-*d*₆): δ 13.29 (s, 1H), 9.34 (s, 1H), 8.71 (d, *J* = 4.1 Hz, 1H), 8.09 (d, *J* = 7.9 Hz, 1H), 7.91 (ddd, *J* = 7.8, 7.8, 1.8 Hz, 1H), 7.51 (s, 1H), 7.43–7.37 (m, 2H), 3.71–3.67 (m, 1H), 3.34–3.29 (m, 2H), 3.18 (d, *J* = 2.7 Hz, 1H), 2.73–2.64 (m, 2H), 1.98–1.91 (m, 4H), 1.42–1.35 (m, 4H). ¹³C NMR (DMSO-*d*₆): δ 160.8, 158.2, 156.0, 152.7, 150.0, 144.3, 137.4, 125.4 (q, *J*_{CF} = 129 Hz), 123.8, 120.1, 52.0, 49.0, 45.4, 33.1 (2C), 31.1 (2C), 29.0 (q, *J* = 30.0 Hz). MS (ES⁺) *m/z* 470.0 [M + H]⁺.

3,3,3-Trifluoro-N-(trans-4-((3-morpholino-1H-pyrazolo[3,4-d]pyrimidin-6-yl)amino)cyclohexyl)propane-1-sulfonamide 21. **21** was obtained by an analogous method to **1** (5.27 g, 11 mmol, 81% yield). ¹H NMR (DMSO-*d*₆): δ 11.98 (bs, 1H), 8.82 (s, 1H), 7.35 (d, *J* = 7.5 Hz, 1H), 7.19 (s, 1H), 3.76 (m, 4H), 3.62 (bs, 1H), 3.33–3.30 (m, 6H), 3.16 (bs, 1H), 2.72–2.62 (m, 2H), 1.93 (m, 4H), 1.40–1.28 (m, 4H). HRMS (ES⁺): *m/z* [M + H]⁺ calcd for C₁₈H₂₇F₃N₇O₃S 478.1843, found 478.1821.

(S)-(2,4-Dichloropyrimidin-5-yl)(2-methylmorpholino)methanone 26a. A solution of (*S*)-2-methylmorpholine (141 g, 1.39 mol) and TEA (141.1 g, 1.4 mol) in DCM (1 L) was added dropwise to a stirred solution of 2,4-dichloropyrimidine-5-carbonyl chloride (268 g, 1.3 mol) in dry DCM (3000 mL) at 0 °C under N₂. The reaction mixture was stirred for 3 h at 0 °C and then quenched with H₂O (500 mL). The phases were separated, and the aqueous phase was extracted with DCM (2 × 300 mL). The combined organic phases were washed with 0.5 M HCl (1 L) and brine (2 L), dried over Na₂SO₄, and then evaporated under reduced pressure. The residue was purified by flash column chromatography (petroleum/EtOAc 20/1 to 1/1) to give **26a** as a yellow oil (188 g, 684 mmol, 53% yield). ¹H NMR (DMSO-*d*₆): δ 8.86 (s, 1H), 4.33–4.25 (m, 1H), 3.95–3.68 (m, 1H), 3.58–3.37 (m, 3H), 3.17–2.64 (m, 2H), 1.20–0.98 (m, 3H). MS (ES⁺) *m/z* 276.0 [M + H]⁺.

(S)-(2-Chloro-4-methoxyppyrimidin-5-yl)(2-methylmorpholino)methanone 27a. Sodium methoxide (40.5 g, 748.9 mmol) was added in portions to a stirred solution of **26a** (188 g, 680.9 mmol) in dry THF (2 L) at –40 °C under N₂. The reaction mixture was stirred for 1 h at –40 °C, and further sodium methoxide (9.2 g, 170.2 mmol) was added

in one portion. The reaction mixture was stirred at $-40\text{ }^{\circ}\text{C}$ for 1 h and gradually warmed to $-10\text{ }^{\circ}\text{C}$ for 1 h. The reaction mixture was quenched with satd aq soln ammonium chloride (500 mL) at $5\text{--}10\text{ }^{\circ}\text{C}$ and extracted with EtOAc ($3 \times 500\text{ mL}$). The combined organic phases were washed with brine (1 L), dried over Na_2SO_4 , and evaporated under reduced pressure. The resulting crude material was purified by flash column chromatography (petroleum ether/EtOAc from 20/1 to 1/1) to give two fractions of **27a** (75 g, 277 mmol, 38% yield and 30 g, 111 mmol, 14% yield) as a yellow oil. This material was used in the next step without further purification.

3,3,3-Trifluoro-N-(trans-4-((4-methoxy-5-((S)-2-methylmorpholine-4-carbonyl)pyrimidin-2-yl)amino)cyclohexyl)propane-1-sulfonamide 28a. To a solution of **27a** (75 g, 276 mmol) in dry dioxane (1500 mL) was added DIPEA (178.4 g, 1.4 mol) and **10b** (139.4 g, 358.8 mmol) in one portion at $27\text{ }^{\circ}\text{C}$. The resulting mixture was stirred at $120\text{ }^{\circ}\text{C}$ for 16 h. The mixture was cooled to room temperature and water (800 mL) and EtOAc (500 mL) added. The reaction mixture was stirred for 10 min, then the organic phase was separated and the aqueous layer was extracted with more EtOAc ($2 \times 500\text{ mL}$). The combined organic phases were washed with brine (2 L), dried over Na_2SO_4 , and filtered. The solvent was removed under vacuum to afford crude material which was purified by flash column chromatography (DCM/MeOH 50/1 to 20/1) to afford **28a** (100 g, 196 mmol, 71% yield) as a pale solid. $^1\text{H NMR}$ (DMSO- d_6): δ 8.03 (s, 1H), 7.49–7.31 (m, 2H), 3.91–3.60 (m, 5H), 3.48–3.11 (m, 9H), 2.68–2.62 (m, 2H), 1.98–1.96 (m, 4H), 1.43–1.09 (m, 7H).

3,3,3-Trifluoro-N-(trans-4-((4-methoxy-5-((S)-2-methylmorpholine-4-carbonothioyl)pyrimidin-2-yl)amino)cyclohexyl)propane-1-sulfonamide 29a. **28a** (117 g, 230 mmol) was dissolved in dry THF (1700 mL). Lawesson's reagent (162.5 g, 401.8 mmol) was added in portions, and the resulting mixture was stirred for 2 h at $45\text{ }^{\circ}\text{C}$. The reaction mixture was cooled to room temperature and quenched by addition of satd aq NaHCO_3 (800 mL). The reaction mixture was stirred for 10 min at RT and then extracted with EtOAc ($3 \times 500\text{ mL}$). The combined organic phases were washed with brine (1 L) and dried over Na_2SO_4 . The solvent was removed under vacuum to afford a crude product which was purified by flash column chromatography (DCM/MeOH 100/1 to 20/1) to afford **29a** (91 g, 173 mmol, 74% yield) as a green solid. $^1\text{H NMR}$ (DMSO- d_6): δ 8.11–8.04 (m, 1H), 7.48–7.31 (m, 2H), 5.34–5.11 m, 1H), 3.96–2.84 (m, 13H), 2.73–2.59 (m, 2H), 2.00–1.78 (m, 4H), 1.44–1.27 (s, 4H), 1.21–1.02 (m, 3H).

2-Methyl-N-(trans-4-((3-morpholino-1H-pyrazolo[3,4-d]pyrimidin-6-yl)amino)cyclohexyl)propane-1-sulfonamide 30. **30** was obtained by an analogous method to **1** (4g, 9.1 mmol, 34% yield). $^1\text{H NMR}$ (DMSO- d_6): δ 12.04 (s, 1H), 8.86 (s, 1H), 7.22 (s, 1H), 7.07–7.00 (m, 1H), 3.85–3.74 (m, 4H), 3.73–3.62 (m, 1H), 3.41–3.31 (m, 4H), 3.18–3.09 (m, 1H), 2.99–2.90 (m, 2H), 2.19–2.10 (m, 1H), 2.03–1.92 (m, 4H), 1.43–1.33 (m, 4H), 1.08 (d, $J = 5.8\text{ Hz}$, 6H). $^{13}\text{C NMR}$ (DMSO- d_6): δ 160.5, 157.3, 154.0, 151.5, 66.2 (2C), 60.5, 51.9, 48.9 (2C), 48.7, 33.3 (2C), 31.3 (2C), 25.0, 22.8 (2C). HRMS (ES^+): m/z [$\text{M} + \text{H}$] $^+$ calcd for $\text{C}_{19}\text{H}_{32}\text{N}_7\text{O}_3\text{S}$ 438.2282, found 438.2262.

3,3,3-Trifluoro-N-(trans-4-((4-methoxy-3-(2-methoxyphenyl)-1H-pyrazolo[3,4-d]pyrimidin-6-yl)amino)cyclohexyl)propane-1-sulfonamide 31. To **44a** (5.95 g, 9.7 mmol) was added 1.25 M HCl in MeOH (450 mL) and the resulting mixture stirred at $60\text{ }^{\circ}\text{C}$ for 30 min. The reaction mixture was concentrated under vacuum to a final volume of 100 mL, satd aq NaHCO_3 (300 mL) added, and extracted with EtOAc (400 mL). The aqueous layer was extracted twice with EtOAc, and the combined organic layers dried over Na_2SO_4 and evaporated under vacuum to obtain crude material which was purified by flash column chromatography (10–90% EtOAc in cyclohexane) to give **31** (3.5 g, 9.7 mmol, 68% yield). $^1\text{H NMR}$ (DMSO- d_6): δ 12.88 (s, 1H), 7.29–7.43 (m, 3H), 7.09 (d, 1H), 6.94–7.03 (m, 2H), 3.83 (s, 3H), 3.62–3.75 (m, 4H), 3.26–3.31 (m, 2H), 3.17 (s, 1H), 2.59–2.73 (m, 2H), 1.87–2.01 (m, 4H), 1.27–1.44 (m, 4H). $^{13}\text{C NMR}$ (DMSO- d_6): δ 164.1, 160.5, 159.7, 158.1, 142.0, 131.1, 130.2, 126.2 (q, $J_{\text{CF}} = 127\text{ Hz}$), 123.5, 120.4, 111.8, 95.8, 55.7, 53.5, 52.0, 49.0, 45.5, 33.2 (2C), 31.3 (2C), 28.9 (q, $J_{\text{CF}} = 29.9\text{ Hz}$). $^{19}\text{F NMR}$ (DMSO- d_6): δ -64.3.

HRMS (ES^+): m/z [$\text{M} + \text{H}$] $^+$ calcd for $\text{C}_{22}\text{H}_{28}\text{F}_3\text{N}_6\text{O}_4\text{S}$ 529.1840, found 529.1822.

N-(trans-4-((4-Methoxy-3-morpholino-1H-pyrazolo[3,4-d]pyrimidin-6-yl)amino)cyclohexyl)-2-methylpropane-1-sulfonamide 33. **44c** (2.63 g, 4.71 mmol) was dissolved in methanolic HCl solution (218 mL, 1.25 M) and stirred at $55\text{ }^{\circ}\text{C}$ for 1 h. The mixture was concentrated under vacuum and EtOAc added and washed with saturated NaHCO_3 solution. The organic phase was washed with brine, dried over Na_2SO_4 , and evaporated under vacuum to give crude product which was purified by flash chromatography (DCM/EtOAc/MeOH 60/30/10) to give **33** (1.82 g, 3.92 mmol, 83% yield). $^1\text{H NMR}$ (DMSO- d_6): δ 11.98 (bs, 1H), 6.98 (d, $J = 7.6\text{ Hz}$, 1H), 6.91 (d, $J = 7.4\text{ Hz}$, 1H), 3.93 (s, 3H), 3.72–3.70 (m, 4H), 3.67–3.57 (m, 1H), 3.22–3.20 (m, 4H), 3.10–3.02 (m, 1H), 2.90 (d, $J = 6.4\text{ Hz}$, 2H), 2.11–2.04 (m, 1H), 1.95–1.87 (m, 4H), 1.38–1.26 (m, 4H), 1.04–1.00 (d, $J = 6.7\text{ Hz}$, 6H). $^{13}\text{C NMR}$ (DMSO- d_6): δ 162.9, 160.6, 160.2, 151.7, 87.3, 66.3 (2C), 60.5, 53.8, 51.9, 49.9 (2C), 33.4 (2C), 31.1 (2C), 25.0, 22.8 (2C). HRMS (ES^+): m/z [$\text{M} + \text{H}$] $^+$ calcd for $\text{C}_{20}\text{H}_{34}\text{F}_3\text{N}_7\text{O}_4\text{S}$ 468.2387, found 468.2367.

N-(trans-4-((4-Methoxy-3-((R)-3-methylmorpholino)-1H-pyrazolo[3,4-d]pyrimidin-6-yl)amino)cyclohexyl)-2-methylpropane-1-sulfonamide 39. **39** was obtained by an analogous method to **33** (33g, 68.8 mmol, 78% yield). $^1\text{H NMR}$ (DMSO- d_6): δ 11.96 (bs, 1H), 6.98 (d, $J = 7.4\text{ Hz}$, 1H), 6.90 (d, $J = 7.4\text{ Hz}$, 1H), 3.99–3.93 (m, 1H), 3.91 (s, 3H), 3.79–3.70 (m, 2H), 3.64–3.51 (m, 3H), 3.27–3.09 (m, 2H), 3.08–3.01 (m, 1H), 2.88 (d, $J = 6.4\text{ Hz}$, 2H), 2.06 (sept, $J = 6.6\text{ Hz}$, 1H), 1.93–1.85 (m, 4H), 1.36–1.26 (m, 4H), 1.04–0.99 (m, 9H). $^{13}\text{C NMR}$ (DMSO- d_6): δ 163.0, 160.4, 160.0, 150.8, 87.5, 71.0, 66.6, 60.5, 53.8, 51.9, 51.1, 49.0, 44.3, 33.3 (2C), 31.4 (2C), 26.8, 25.0, 22.8 (2C), 12.9. HRMS (ES^+): m/z [$\text{M} + \text{H}$] $^+$ calcd for $\text{C}_{21}\text{H}_{36}\text{N}_7\text{O}_4\text{S}$ 482.2544, found 482.2523. Enantiopurity determined using a chiral column: 250 mm Chiralpak IA, 150 mm \times 4.6 mm 5 μm , heptane/EtOH = 65/35 + 0.2% *iso*-propyl amine, 1.0 mL/min, 298 K, 254 nm. First enantiomer (**39**, only peak detected) $R_t = 8.5\text{ min}$, second enantiomer (compound **40**, not detected) $R_t = 15.5\text{ min}$. *ee* measured: 100%.

3-Bromo-4,6-dichloro-1-(tetrahydro-2H-pyran-2-yl)-1H-pyrazolo[3,4-d]pyrimidine 41a. A solution of 3-bromo-4,6-dichloro-1H-pyrazolo[3,4-d]pyrimidine (40 g, 149 mmol), 3,4-dihydro-2H-pyran (41 mL, 447 mmol), and *p*-toluenesulfonic acid monohydrate (5.7 g, 30 mmol) in THF (650 mL) was stirred at $70\text{ }^{\circ}\text{C}$ for 2 h. After cooling, the solvent was evaporated, ether (200 mL) added, and the resulting suspension stirred for 2 h at $40\text{ }^{\circ}\text{C}$, slowly cooled, and the resulting solid collected, washed with ether, and dried to give **41a** (41.5 g, 118 mmol, 79% yield). $^1\text{H NMR}$ (CDCl_3 - d_6): δ 6.00 (dd, $J = 2.6$ and 6.0 Hz , 1H), 4.18–4.10 (m, 1H), 3.84–3.76 (m, 1H), 2.62–2.49 (m, 1H), 2.20–2.13 (m, 1H), 1.86–1.63 (m, 4H). MS (ES^+) m/z 349.0, 351.0, 353.0 [$\text{M} + \text{H}$] $^+$.

3-Bromo-4,6-dichloro-1-((2-(trimethylsilyl)ethoxy)methyl)-1H-pyrazolo[3,4-d]pyrimidine 41b. A solution of 3-bromo-4,6-dichloro-1H-pyrazolo[3,4-d]pyrimidine (65.5 g, 244 mmol) in DCM (1.5 L) at $0\text{ }^{\circ}\text{C}$ was added DIPEA (125 mL, 733 mmol) dropwise (30 min) and the resulting solution stirred at $0\text{ }^{\circ}\text{C}$ for 5 min. After this time, 2-(trimethylsilyl)ethoxymethyl chloride (51.5 mL, 293 mmol) was added dropwise (40 min) and stirred at $3\text{--}4\text{ }^{\circ}\text{C}$ for 1.5 h. Water (1 L) was added to the reaction and the phases separated. The organic layer was washed with H_2O (1 L), dried over Na_2SO_4 , filtered, and concentrated to give **41b** as a brown solid which was used without purification (101 g, 245 mmol, quant yield). $^1\text{H NMR}$ (DMSO- d_6): δ 5.7 (s, 2H), 3.6 (dd, $J = 8.1, 8.1\text{ Hz}$, 2H), 0.85 (dd, $J = 8.1, 8.1\text{ Hz}$, 2H), 0.95 (s, 9H). MS (ES^+) m/z 395.0, 397.0 [$\text{M} + \text{H}$] $^+$.

3-Bromo-6-chloro-4-methoxy-1-(tetrahydro-2H-pyran-2-yl)-1H-pyrazolo[3,4-d]pyrimidine 42a. To **41a** (35.8 g, 102 mmol) in MeOH (160 mL) was added a solution of sodium methoxide (5.5 g, 102 mmol) in MeOH (500 mL) dropwise over 1 h and the resulting suspension stirred for 30 min. Solvent was evaporated, EtOAc added and washed with satd aq NaHCO_3 , then dried over sodium sulfate and solvent evaporated to give **42a** which was used without purification (35.5 g). $^1\text{H NMR}$ (DMSO- d_6): δ 5.84 (dd, $J = 2.5$ and 5.8 Hz , 1H), 4.14 (s, 3H), 3.99–3.93 (m, 1H), 3.73–3.68 (m, 1H), 2.35–2.26 (m, 1H), 2.03–

1.96 (m, 1H), 1.93–1.87 (m, 1H), 1.80–1.72 (m, 1H), 1.60–1.53 (m, 2H). MS (ES⁺) *m/z* 347, 349 [M + H]⁺.

3-Bromo-6-chloro-4-methoxy-1-((2-(trimethylsilyl)ethoxy)methyl)-1H-pyrazolo[3,4-d]pyrimidine 42b. To **41b** (772 g, 1.94 mol) in MeOH (20 L) was added sodium methoxide (115.2 g, 2.13 mol) in MeOH (230 mL) dropwise and the resulting solution stirred at room temperature for 30 min. The reaction mixture was partitioned between EtOAc (10 L) and brine (2 L) and the organic layer separated, washed with brine (2 L), dried over Na₂SO₄, filtered, and concentrated. This residue was purified by column chromatography on silica gel (100–200 mesh silica gel) eluted with petroleum ether:EtOAc (100:1–100:2) to give a crude product. This crude product was purified by recrystallization from petroleum ether (1 L) to give **42b** as a white solid (450 g, 1.14 mol, 58.8% yield). ¹H NMR (DMSO-*d*₆): δ 5.62 (s, 2H), 4.14 (s, 3H), 3.59 (t, *J* = 8.2 Hz, 2H), 0.84 (t, *J* = 8.1 Hz, 2H), 0.07 (s, 9H). MS (ES⁺) *m/z* 392.9, 395.0 [M + H]⁺.

N-(trans-4-((3-Bromo-4-methoxy-1-(tetrahydro-2H-pyran-2-yl)-1H-pyrazolo[3,4-d]pyrimidin-6-yl)amino)cyclohexyl)-2-methylpropane-1-sulfonamide 43a. To a stirred solution of **42a** (7.82 g, 22.44 mmol) and **10a** (6 g, 17.26 mmol) in ethanol (172 mL) was added DIPEA (12 mL, 69.04 mmol) and the mixture heated to 70 °C and stirred for 2 days. Solvent was evaporated and the crude material purified by flash chromatography (30–50% ethyl acetate/cyclohexane) to afford **43a** (5.5 g, 10.1 mmol, 58% yield). ¹H NMR (DMSO-*d*₆): δ 7.52 (dd, *J* = 9.5, 17.0 Hz, 1H), 7.04 (d, *J* = 7.6 Hz, 1H), 5.65–5.55 (m, 1H), 4.05–3.96 (m, 2H), 3.67 (s, 2H), 3.33 (s, 3H), 2.92–2.89 (m, 2H), 2.36–2.27 (m, 1H), 2.13–2.06 (m, 1H), 1.94 (s, 3H), 1.83 (dd, *J* = 13.2, 13.2 Hz, 1H), 1.54 (s, 2H), 1.36 (d, *J* = 18.6 Hz, 6H), 1.05–1.01 (m, 6H). MS (ES⁺) *m/z* 547.3, 545.3 [M + H]⁺.

3,3,3-Trifluoro-N-(trans-4-((4-methoxy-3-(2-methoxyphenyl)-1-((2-(trimethylsilyl) ethoxy)methyl)-1H-pyrazolo[3,4-d]pyrimidin-6-yl)amino)cyclohexyl)propane-1-sulfonamide 44a. To **43b** (3.9 g, 6.6 mmol) and 2-methoxyphenylboronic acid (1.37 g, 8.9 mmol) was added [1,1'-bis(diphenylphosphino)ferrocene]palladium(II) dichloride (483 mg, 0.66 mmol), sodium carbonate (2.1 g, 39.6 mmol), DME (160 mL), and H₂O (80 mL) under argon. The resulting mixture was stirred at 110 °C for 30 min. The reaction mixture was filtered then concentrated under vacuum. The residue was taken up in EtOAc and washed with a satd aq soln NH₄Cl. The layers were separated and the organic phase washed with brine, dried over Na₂SO₄, and concentrated. The crude material was purified by flash column chromatography (6:4 cyclohexane in EtOAc) to afford **44a** which was used without further purification (4.04 g, 6.6 mmol, quant yield). MS (ES⁺) *m/z* 613.3 [M + H]⁺.

3,3,3-Trifluoro-N-(trans-4-((4-methoxy-3-morpholino-1-(tetrahydro-2H-pyran-2-yl)-1H-pyrazolo[3,4-d]pyrimidin-6-yl)amino)cyclohexyl)propane-1-sulfonamide 44b. A mixture of **43b** (0.25 g, 0.43 mmol), morpholine (0.186 mL, 2.14 mmol), cesium carbonate (0.39 g, 1.20 mmol), 4,5-bis(diphenylphosphino)-9,9-dimethylxanthene (0.03 g, 0.05 mmol), and palladium acetate (9.6 mg, 0.043 mmol) in 1,4-dioxane (4.08 mL) was purged with argon and heated at 110 °C overnight. The resulting mixture was partitioned between ethyl acetate (75 mL) and water (150 mL). The phases were separated and the aqueous phase extracted with ethyl acetate (1 × 75 mL). The organic phases were combined with two further additional experiments, dried with Na₂SO₄, filtered, and concentrated to give **44b** as a brown oil (250 mg, 0.42 mmol, 45% overall yield from all three experiments) which was used without purification. MS (ES⁺) *m/z* 592.2 [M + H]⁺.

N-(trans-4-((4-Methoxy-3-morpholino-1-(tetrahydro-2H-pyran-2-yl)-1H-pyrazolo[3,4-d]pyrimidin-6-yl)amino)cyclohexyl)-2-methylpropane-1-sulfonamide 44c. The reaction was run in two batches: To a mixture of **43a** (2.6 g, 4.8 mmol), sodium *tert*-butoxide (1.4 g, 14.3 mmol), xantphos (0.66 g, 1.14 mmol), and Pd₂ dba₃ (0.436 g, 0.48 mmol) in dioxane (160 mL) was added morpholine (4.16 mL, 47.6 mmol) and the mixture heated at 110 °C for 30 min. The reaction mixture was filtered through Celite, then diluted with ethyl acetate and washed with satd NH₄Cl. The aqueous phase was extracted with ethyl acetate, washed with brine, dried over Na₂SO₄, filtered, and evaporated. The crude material from both batches was combined and purified by flash chromatography (50–80% EtOAc/cyclohexane) to give **44c** (2.6 g, 4.7 mmol, 49% overall yield from both experiments). ¹H NMR

(DMSO-*d*₆): δ 7.18–7.09 (m, 1H), 7.00 (d, *J* = 8.0 Hz, 1H), 5.55–5.49 (m, 1H), 4.00–3.91 (m, 4H), 3.78–3.64 (m, 5H), 3.58–3.50 (m, 1H), 3.30–3.22 (m, 4H), 3.11–3.05 (m, 1H), 2.91 (d, *J* = 6.4 Hz, 2H), 2.42–2.31 (m, 1H), 2.09 (sept, *J* = 6.7 Hz, 1H), 2.03–1.89 (m, 5H), 1.80–1.62 (m, 2H), 1.55–1.50 (m, 2H), 1.41–1.30 (m, 4H), 1.04 (d, *J* = 6.7 Hz, 6H). MS (ES⁺) *m/z* 552.5 [M + H]⁺.

(S)-N-trans-4-((4-Methoxy-3-(3-methylmorpholino)-1-((2-(trimethylsilyl)ethoxy)methyl)-1H-pyrazolo[3,4-d]pyrimidin-6-yl)amino)cyclohexyl)-2-methylpropane-1-sulfonamide 44e. A mixture of **43d** (35 g, 59.2 mmol) in 1,4-dioxane (1000 mL) was purged with argon, (R)-3-methylmorpholine (59.8 g, 592 mmol), Tris-(dibenzylideneacetone)dipalladium(0) (5.42 g, 5.92 mmol), and dicyclohexyl(2',6'-diisopropoxy-[1,1'-biphenyl]-2-yl)phosphine (5.52 g, 11.83 mmol) added and purged with argon. Potassium bis(trimethylsilyl)amide (0.5 M in toluene, 237 mL, 118 mmol) was added and purged and the mixture stirred at 110 °C for 2 h. The crude mixture was cooled, filtered through Celite, partitioned between ethyl acetate (500 mL) and brine (1 L), the phases separated, and the organic phase washed with further brine (1 L). The combined aqueous layers were extracted with ethyl acetate (1 L) and the organic layers combined, dried over Na₂SO₄, filtered, and concentrated. Crude material was purified by flash chromatography (cyclohexane/EtOAc gradient 0–30%) to give **44e** as a brown solid (16.91 g, 27.6 mmol, 47%). ¹H NMR (DMSO-*d*₆): δ 7.20–7.10 (m, 1H), 7.04–6.96 (m, 1H), 5.35–5.25 (m, 2H), 4.05–3.90 (m, 4H), 3.82–3.63 (m, 3H), 3.61–3.49 (m, 3H), 3.26–3.15 (m, 2H), 3.09–3.03 (m, 1H), 2.89 (d, *J* = 6.4 Hz, 2H), 2.07 (sept, *J* = 6.7 Hz, 1H), 1.95–1.86 (m, 3H), 1.38 (s, 3H), 1.36–1.28 (m, 3H), 1.04 (d, *J* = 6.6 Hz, 3H), 1.00 (d, *J* = 6.7 Hz, 6H), 0.84–0.76 (m, 2H), –0.10 (s, 9H). MS (ES⁺) *m/z* 612.3 [M + H]⁺.

Intramacrophage Leishmania donovani Assay. This assay was conducted as previously described.¹⁴

Kinetic Aqueous Solubility Assessment.²³ The aqueous solubility of test compounds were measured using an in-house method utilizing quantification via chemiluminescent nitrogen detection (CLND): a 5 μL of 10 mM DMSO stock solution was diluted to 100 μL with pH 7.4 phosphate buffered saline and equilibrated for 1 h at RT, filtered through Millipore Multiscreen HTS-PCF filter plates (MSSL BPC). The eluent is quantified by suitably calibrated flow injection CLND. This assay has a dynamic range between the lower detection limit of 1 and 500 μM, governed by the protocol's 1:20 dilution into pH 7.4 phosphate buffer solution from nominal 10 mM DMSO stock.

Solubility of Solid Compounds in Fasted Simulated Intestinal Fluid.³² Solubility of test compounds in fasted simulated intestinal fluid (FaSSIF) were determined at pH 6.5 after 4 h equilibration at room temperature. One mL of FaSSIF buffer (3 mM sodium taurocholate, 0.75 mM lecithin in sodium phosphate buffer at pH 6.5) was added to manually weighed 1 mg of solid compound in a 2 mL HPLC autosampler vial. The resulting suspension is shaken at 900 rpm for 4 h at room temperature and then transferred to a Multiscreen HTS, 96-well solubility filter plate. The residual solid was removed by filtration. The supernatant solution was quantified by HPLC-UV using single-point calibration of a known concentration of the compound in DMSO. The dynamic range of the assay was 1–1000 μg/mL.

Measurement of ChromLogD.^{23,31} The chromatographic hydrophobicity index (CHI)⁴⁵ values are measured using reversed phase HPLC column (50 mm × 2 mm 3 μM Gemini NX C18, Phenomenex, UK) with fast acetonitrile gradient at starting mobile phase of pHs 2, 7.4, and 10.5. CHI values are derived directly from the gradient retention times by using a calibration line obtained for standard compounds. The CHI value approximated the volume% organic concentration when the compound was eluted. CHI is linearly transformed into ChromLogD^{23,31} by least-squares fitting of experimental CHI values to calculated ClogP values for over 20K research compounds using the following formula: ChromlogD = 0.0857 × CHI - 2.00.

Stability in Microsomes. Test compound (0.5 μM) was incubated with either female CD1 mouse (Xenotech) or human (IVT) liver microsomes and their action started with addition of excess NADPH (8 mg/mL 50 mM potassium phosphate buffer, pH 7.4). Immediately, at

time zero, then at 3, 6, 9, 15, and 30 min, an aliquot (50 μL) of the incubation mixture was removed and mixed with acetonitrile (100 μL) to stop the reaction. Internal standard was added to all samples, the samples centrifuged to sediment precipitated protein, and the plates then sealed prior to UPLC-MS/MS analysis using a Quattro Premier XE (Waters Corporation, USA). XLfit (IDBS, UK) was used to calculate the exponential decay and consequently the rate constant (k) from the ratio of the peak area of test compound to internal standard at each time point. The rate of intrinsic clearance (Cl_i) of each test compound was then calculated using the equation Cl_i (mL/min/g liver) = $k \times V \times$ microsomal protein yield, where V (mL/mg protein) is the incubation volume/mg protein added and microsomal protein yield is taken as 52.5 mg protein/g liver. Verapamil (0.5 μM) was used as a positive control to confirm acceptable assay performance.

Plasma Protein Binding Experiments. In brief, a 96-well equilibrium dialysis apparatus was used to determine the free fraction in mouse plasma for each compound (HT Dialysis LLC, Gales Ferry, CT). Membranes (12–14 kDa a cutoff) were conditioned in deionized water for 60 min, followed by conditioning in 80:20 deionized water:ethanol for 20 min and then rinsed in isotonic buffer before use. Female CD1 mouse plasma was removed from the freezer and allowed to thaw on the day of experiment. Thawed plasma was then centrifuged (Allegra X12-R, Beckman Coulter, USA), spiked with test compound (final concentration 10 $\mu\text{g}/\text{mL}$), and 150 μL aliquots ($n = 6$ replicate determinations) loaded into the 96-well equilibrium dialysis plate. Dialysis vs isotonic buffer (150 μL) was carried out for 5 h in a temperature controlled incubator at ca. 37 $^\circ\text{C}$ (Barworld scientific Ltd., UK) using an orbital microplate shaker at 100 rpm (Barworld scientific Ltd., UK). At the end of the incubation period, 50 μL aliquots of plasma or buffer were transferred to micronic tubes (Micronic BV, The Netherlands) and the composition in each tube balanced with control fluid (50 μL), such that the volume of buffer to plasma was the same. Sample extraction was performed by the addition of 200 μL of acetonitrile containing an appropriate internal standard. Samples were allowed to mix for 1 min and then centrifuged at 3000 rpm in 96-well blocks for 15 min (Allegra X12-R, Beckman Coulter, USA), after which 150 μL of supernatant was removed to 50 μL of water. All samples were analyzed by UPLC-MS/MS on a Quattro Premier XE mass spectrometer (Waters Corporation, USA). The unbound fraction was determined as the ratio of the peak area in buffer to that in plasma.

Melting Point (mtp) Determination. Determination of melting point of compounds were measured by thermal analysis, performing differential scanning calorimetry, (DSC) experiments, which measured temperatures and heat flows associated with thermal transitions in a material. The equipment utilized was from TA Instruments (Q20, RCS Refrigerator), using the system Software Q Advantage for Q Series and Analysis Software TA universal analysis.

As general operating conditions, the following were set up: start temperature 25 $^\circ\text{C}$, end temperature 350 $^\circ\text{C}$, heating rate 10 $^\circ\text{C}/\text{min}$. The sample quantity ranged from 1 to 3 mg, placed in a hermetic pan. The corresponding analysis with the thermal transitions occurred was obtained based on a reference blank sample (empty pan) to get the difference between the sample and the reference in the energy response when heating equally both pans.

pK_a Determination.³⁵ The Sirius T3 (Sirius Analytical Inc., UK) instrument has been used for pK_a determination of the compounds. The pK_a determination is based on acid–base titration, and the protonation/deprotonation of the molecule is measured either by UV spectroscopy or potentiometrically. The pK_a value is calculated from the pH, where the 50–50% of the protonated and unprotonated form of the molecules are present.

The UV-metric method provides pK_a results for samples with chromophores whose UV absorbance changes as a function of pH. It typically required 5 μL of a 10 mM solution of the samples, and the UV absorbance was monitored over 54 pH values in a buffered solution in about 5 min.

When the ionization center was far from the UV, the chromophore pH-metric method based on potentiometric acid–base titration was used. The pH of each point in the titration curve was calculated using equations that contain pK_a , and the calculated points were fitted to the

measured curve by manipulating the pK_a . The pK_a that provided the best fit was taken to be the measured pK_a .

Usually 0.5–1 mg of solid material is required for the measurements. When the compound precipitated at some point during the pH titration, the cosolvent method using methanol was applied using various concentration of cosolvent. The pK_a in water was calculated using the Yasuda–Shedlovsky extrapolation method.

X-ray Diffraction Studies of 1 and 15. Data for both studies were collected with an Oxford Diffraction Gemini A Ultra diffractometer at 150(2) K using Cu $K\alpha$ X-radiation ($\lambda = 1.54178 \text{ \AA}$).

Crystal Data and Refinement Summary for 1. $\text{C}_{19}\text{H}_{28}\text{F}_3\text{N}_7\text{O}_3\text{S}$; $M = 491.54$; colorless tablet from the slow evaporation of a solution of **1** in DMSO and 1-butanol; 0.32 mm \times 0.15 mm \times 0.07 mm; triclinic; space group $P1$ (#1); $a = 8.68517(18) \text{ \AA}$, $b = 16.0121(3) \text{ \AA}$, $c = 17.5996(4) \text{ \AA}$, $\alpha = 95.8623(16)^\circ$, $\beta = 102.6295(18)^\circ$, $\gamma = 100.2962(16)^\circ$, $V = 2324.30(8) \text{ \AA}^3$; $Z = 4$; $D_{\text{calc}} = 1.405 \text{ Mg m}^{-3}$; $\theta_{\text{max}} = 67.03^\circ$; reflections collected = 33974; independent reflections = 33974; $R_{\text{int}} = 0.0000$ (HKLF 5 treatment owing to crystal splitting); coverage = 99.2%; restraints = 896; parameters = 1395; $S = 1.041$; $R_1 [I > 2\sigma(I)] = 0.0526$; wR_2 (all data) = 0.1479; absolute structure parameter = 0.022(9); and largest difference peak and hole = 0.572 and 0.322 e \AA^{-3} .

Crystal Data and Refinement Summary for 15. $\text{C}_{19}\text{H}_{22}\text{F}_3\text{N}_7\text{O}_2\text{S}$; $M = 469.50$; colorless block from the slow evaporation and seeding of a solution of **15** in DMSO and DMF; 0.21 mm \times 0.14 mm \times 0.06 mm; triclinic; space group $P1$ (#2); $a = 8.5590(2) \text{ \AA}$, $b = 8.6492(2) \text{ \AA}$, $c = 14.0372(4) \text{ \AA}$, $\alpha = 85.196(2)^\circ$, $\beta = 89.219(2)^\circ$, $\gamma = 85.087(2)^\circ$, $V = 1031.68(4) \text{ \AA}^3$; $Z = 2$; $D_{\text{calc}} = 1.511 \text{ Mg m}^{-3}$; $\theta_{\text{max}} = 66.74^\circ$; reflections collected = 22081; independent reflections = 3644; $R_{\text{int}} = 0.0351$; coverage = 99.4%; restraints = 0; parameters = 301; $S = 1.048$; $R_1 [I > 2\sigma(I)] = 0.0346$; wR_2 (all data) = 0.0956; and largest difference peak and hole = 0.253 and 0.454 e \AA^{-3} .

A description of the refinements and the full tables associated with the crystal structures are given in the [Supporting Information](#). Crystallographic information files have been deposited with the Cambridge Crystallographic Data Centre. CCDC 1857125 (**1**) and 1857128 (**15**) contain the supplementary crystallographic data for this paper. The data can be obtained free of charge from The Cambridge Crystallographic Data Centre via www.ccdc.cam.ac.uk/structures.

In Vivo Pharmacokinetics. Mouse. Test compound **15** was dosed intravenously or orally by gavage as a solution at 3 or 10 mg free base/kg respectively (dose volume, 5 or 10 mL/kg respectively; dose vehicle, 10% (v/v) dimethyl sulfoxide (DMSO), 60% polyethylene glycol 400, and 30% deionized water) to female Balb/c mice ($n = 3$). Blood samples were taken from each mouse at 0.08, 0.25, 0.5, 1, 2, 4, 6, 8, and 24 h post dose and mixed with two volumes of distilled water. After suitable sample preparation, the concentration of test compound in blood was determined by UPLC-MS/MS using a Quattro Premier XE (Waters, USA). Pharmacokinetic parameters were derived from the mean blood concentration time curve using PK solutions software v 2.0 (Summit Research Services, USA).

Rat. Male Sprague–Dawley rats ($n = 3$) were dosed with **1**, **30**, **31**, **33**, and **39** either intravenously at a target dose of 1 mg/kg or orally at a target dose of 10, 100, and 300 mg/kg.

Following discrete intravenous tail vein dosing from a solution of 5% DMSO:20% Encapsin in saline, serial blood samples ($\sim 200 \mu\text{L}$) were taken via lateral tail vein at 0.08, 0.25, 0.5, 1, 2, 4, 8, and 24 h post dose and placed into individual tubes containing potassium EDTA and thoroughly mixed. Blood samples were placed on ice immediately after collection. Within 2 h of collection, 70 μL of blood sample was transferred to a tube containing 130 μL of 0.1N Hepes buffer. Following dilution, samples were stored at approximately -20°C or below until analysis.

Following discrete oral gavage dosing from a suspension of 1% methyl cellulose at target doses of 10, 100, and 300 mg/kg, respectively, serial blood samples ($\sim 200 \mu\text{L}$) were taken via lateral tail vein at 0.25, 0.5, 0.75, 1, 2, 4, 6, 8, and 24 h post dose and placed into individual tubes containing potassium EDTA and thoroughly mixed. Blood samples were placed on ice immediately after collection. Within 2 h of collection, 70 μL of blood sample was transferred to a tube containing

130 μL of 0.1N Hepes buffer. Following dilution, samples were stored at approximately $-20\text{ }^\circ\text{C}$ or below until analysis.

Samples were analyzed for parent using a method based on protein precipitation followed by LCMS/MS with a quantitative range between 2.90 and 2860 ng/mL.

Once analyzed, if concentrations were above the dynamic range of the standard curve, prediluted samples were diluted with blank matrix (1:2.86 whole blood:0.1N Hepes buffer) and processed normally for analysis.

Data Analysis. Data analysis and calculation of pharmacokinetic parameters was performed using Phoenix, WinNonLin version 6.3.

Following the intravenous administration, the whole blood clearance (Cl) was calculated by determining the dose administered to each animal and dividing by the $\text{AUC}_{0-\infty}$. The estimate of the volume of distribution at steady state (V_{ss}) was calculated as $\text{MRT} \times \text{Cl}$, where MRT is the mean residence time, calculated by $\text{AUMC}_{0-\infty}/\text{AUC}_{0-\infty}$.

For both intravenous and oral administration, the systemic exposures were determined by calculating the area under the blood concentration–time curve (AUC) from the start of dosing to the last observed quantifiable concentration (AUC_{0-t}) by using the linear up-log down trapezoidal rule. The slope of the terminal elimination phase was estimated by linear regression of the terminal data points (minimum 3 points) from a natural log concentration vs time plot of the data. The half-life ($t_{1/2}$) of the terminal elimination phase was calculated as $t_{1/2} = 0.693/k$ (where k is the elimination rate constant).

Graphs were generated using Microsoft Excel.

In Vivo Efficacy Studies. Groups of female BALB/c mice (5 per group) were inoculated intravenously with approximately 2×10^7 *L. donovani* amastigotes (LV9; WHO designation: MHOM/ET/67/HU3) harvested from the spleen of an infected hamster.⁴⁶ From day 7 postinfection, groups of mice were treated with either drug vehicle only (orally), with pentostam (15 mg/kg subcutaneously) with miltefosine (12 or 30 mg/kg orally), with compound 15 (50 mg/kg orally), with compound 30 (10, 25, 50, and 100 mg/kg orally), with compound 37 (25 mg/kg orally), or with compounds 1, 31, and 39 (10 and 25 mg/kg orally). Miltefosine was dosed once daily for 5 or 10 days, compound 15 was dosed twice daily for 5 days, compound 30 was dosed twice daily for 5 and 10 days, and compounds 1, 31, 37, and 39 were dosed twice daily for 10 days. Drug dosing solutions were prepared fresh each day and the vehicle was deionized water for miltefosine and pentostam, 10% (v/v) dimethyl sulfoxide (DMSO), 60% polyethylene glycol 400, and 30% deionized water for 15 and 0.5% HPMC, 0.4% Tween 80, and 0.5% benzyl alcohol for 1, 31, 37, and 39. On day 14 (5 days dosing groups) or 19 (10 days dosing groups) all animals were humanely euthanized, liver smears made, and parasite burdens determined by counting the number of amastigotes/500 liver cells. Parasite burden is expressed in Leishman–Donovan units (LDU): the number of amastigotes per 500 nucleated cells multiplied by the organ weight in grammes.³⁰

Preclinical Safety Studies. *Cytochrome P450 Enzyme Isoform 3A4*. CYP3A4 inhibition and metabolism dependent inhibition (MDI) was assessed using a marker substrate (midazolam), monitoring production of CYP3A4 specific metabolite in the presence and absence of test compound at eight concentrations up to 100 μM (0.1 to 100 μM , final organic content $\leq 0.5\%$). Known inhibitors of CYP3A4 were included as positive control (troleandomycin, ketoconazole, and erythromycin). Data quoted as IC_{50} and fold shift in IC_{50} (MDI).

Incubation mixture containing pooled human liver microsomes (final concentration 0.1 mg/mL), and either substrate, standard inhibitor, or test compound was preincubated at $37\text{ }^\circ\text{C}$ for 20 min. Either substrate or cofactor was then added and incubated in plate shaker for another 5 min at $37\text{ }^\circ\text{C}$. Ice-cold acetonitrile 2:1 (v/v) was added to terminate reaction. Depletion of substrates was measured by LC-MS/MS, and pIC_{50} was measured. If a greater than 1.5-fold change in pIC_{50} was observed upon preincubation with cofactor values compared to preincubation with substrate values, this suggests that the test compound is a metabolism dependent inhibitor.

Chemoproteomic Profiling on Kinobeads. This assay was conducted as previously described.¹⁷

Ames. The standard protocol was used for this assay.³⁸

Mouse Lymphoma Assay (MLA). The standard protocol was used for this assay.⁴¹

Human Ether-a-go-go Related Gene (hERG). The standard protocol was used for this assay.^{39,40}

Rat 7-Day Toxicology. Test compounds were administered to male Crl:WI(Han) rats in a 7 day, oral gavage, repeat-dose study at doses of 100, 300, and 1000 mg/kg/day.

Rat Cardiovascular Study. Conscious unrestrained telemetered male rats (CRL:WI (Han)) were given a single oral dose of either vehicle or test article (up to 1000 mg/kg) cardiovascular and electrocardiographic parameters, and body temperature were monitored for 2 h prior to and for 24 h after dose.

Ethical Statements. Mouse and Rat Pharmacokinetics. All animal studies were ethically reviewed and carried out in accordance with Animals (Scientific Procedures) Act 1986 and the GSK/Dundee University Policy on the Care, Welfare, and Treatment of Animals

In Vivo Efficacy. All regulated procedures, at the University of Dundee, on living animals was carried out under the authority of a project license issued by the Home Office under the Animals (Scientific Procedures) Act 1986, as amended in 2012 (and in compliance with EU Directive EU/2010/63). License applications will have been approved by the University's Ethical Review Committee (ERC) before submission to the Home Office. The ERC has a general remit to develop and oversee policy on all aspects of the use of animals on University premises and is a subcommittee of the University Court, its highest governing body.

Rat Toxicology Studies. All animal studies were ethically reviewed and carried out in accordance with Animals (Scientific Procedures) Act 1986 and the GSK Policy on the Care, Welfare, and Treatment of Animals

Human Biological Samples. All were sourced ethically and their research use was in accord with the terms of the informed consents.

■ ASSOCIATED CONTENT

📄 Supporting Information

The Supporting Information is available free of charge on the ACS Publications website at DOI: 10.1021/acs.jmedchem.8b01218.

Chemistry experimental; crystallography; supplementary data table; synthetic details for all compounds (PDF)

Experimental set up and supplementary tables (XLS)

Molecular formula strings (CSV)

■ AUTHOR INFORMATION

Corresponding Authors

*For T.J.M.: phone, +34 650 349771; E-mail, tim.j.miles@gsk.com.

*For K.D.R.: phone, +44 1382 388 688; E-mail, k.read@dundee.ac.uk.

*For P.G.W.: phone, +44 1382 386 231; E-mail, p.g.wyatt@dundee.ac.uk.

ORCID

Manu De Rycker: 0000-0002-3171-3519

Ian H. Gilbert: 0000-0002-5238-1314

Paul G. Wyatt: 0000-0002-0397-245X

Kevin D. Read: 0000-0002-8536-0130

Timothy J. Miles: 0000-0001-7407-7404

Notes

The authors declare the following competing financial interest(s): The following authors have shares in GlaxoSmithKline: M.Bo., R.C.B.C., S.D.C., A.D., G.D., S.F., S.G.-D., S.G., A.P.H., S.J.H., R.L., F.M., V.L.N., I.H.R., T.U., D.G., J.M.F., P.G.W., K.D.R., and T.J.M. The other authors declare no competing interests.

ACKNOWLEDGMENTS

Funding for this work was provided by the Wellcome (nos. 092340 and 100476). We thank Gina MacKay and Daniel Fletcher for performing HRMS analyses and for assistance with performing other NMR and MS analyses, Irene Hallyburton for performing the axenic assay, Raul Fernandez Velasco and the rest of the Galchimia chemistry team plus Colin P. Leslie and the rest of the Aptuit chemistry team for synthesizing key compounds, Professor W. Clegg and Dr. R. W. Harrington plus Dr. M. R. Probert for the GSK-funded crystal structures of **1** and **15**, Alastair Pate and Francesco Gastaldello for data management, and finally Dr. Robert J. Young for critical evaluation of the manuscript.

ABBREVIATIONS USED

THP-1, human monocytic cell line derived from an acute monocytic leukemia patient; HPMC, hydroxypropyl methylcellulose; VL, visceral leishmaniasis; CRK-12, cdc2-related kinase 12

REFERENCES

- (1) World Health Organization (WHO) List of Neglected Tropical Diseases; World Health Organization: Geneva, 2018; http://www.who.int/neglected_diseases/diseases/en/ (accessed Aug 2, 2018).
- (2) Field, M. C.; Horn, D.; Fairlamb, A. H.; Ferguson, M. A. J.; Gray, D. W.; Read, K. D.; De Rycker, M.; Torrie, L. S.; Wyatt, P. G.; Wyllie, S.; Gilbert, I. H. Anti-trypanosomatid drug discovery: an ongoing challenge and a continuing need. *Nat. Rev. Microbiol.* **2017**, *15* (4), 217–231.
- (3) World Health Organization (WHO) Leishmaniasis Fact Sheet; World Health Organization: Geneva, 2018; <http://www.who.int/mediacentre/factsheets/fs375/en/> (accessed Aug 2, 2018).
- (4) Moore, E. M.; Lockwood, D. N. Treatment of visceral leishmaniasis. *J. Glob. Infect. Dis.* **2010**, *2* (2), 151–158.
- (5) Sundar, S.; Singh, A.; Rai, M.; Prajapati, V. K.; Singh, A. K.; Ostyn, B.; Boelaert, M.; Dujardin, J.-C.; Chakravarty, J. Efficacy of Miltefosine in the Treatment of Visceral Leishmaniasis in India After a Decade of Use. *Clin. Infect. Dis.* **2012**, *55* (4), 543–550.
- (6) den Boer, M. L.; Alvar, J.; Davidson, R. N.; Ritmeijer, K.; Balasegaram, M. Developments in the treatment of visceral leishmaniasis. *Expert Opin. Emerging Drugs* **2009**, *14* (3), 395–410.
- (7) Mueller, M.; Ritmeijer, K.; Balasegaram, M.; Koummuki, Y.; Santana, M. R.; Davidson, R. Unresponsiveness to AmBisome in some sudanese patients with kala-azar. *Trans. R. Soc. Trop. Med. Hyg.* **2007**, *101* (1), 19–24.
- (8) Drugs for Neglected Diseases initiative (DNDi) Portfolio; Drugs for Neglected Diseases initiative (DNDi), June 2018; <https://www.dndi.org/diseases-projects/portfolio/> (accessed Oct 5, 2016).
- (9) Drugs for Neglected Diseases initiative (DNDi) Target Product Profile for Visceral Leishmaniasis; Drugs for Neglected Diseases initiative (DNDi), 2016; <https://www.dndi.org/diseases-projects/leishmaniasis/tpp-vl/> (accessed Oct 5, 2016).
- (10) Freitas-Junior, L. H.; Chatelain, E.; Kim, H. A.; Siqueira-Neto, J. L. Visceral leishmaniasis treatment: what do we have, what do we need and how to deliver it? *Int. J. Parasitol.: Drugs Drug Resist.* **2012**, *2*, 11–19.
- (11) Gilbert, I. H. Drug discovery for neglected diseases: molecular target-based and phenotypic approaches. *J. Med. Chem.* **2013**, *56* (20), 7719–7726.
- (12) Palmer, M. J.; Wells, T. N. C.; Eds., *Neglected Diseases and Drug Discovery*. [In: *RSC Drug Discovery Ser.*, 2012; 14; 438]. Royal Society of Chemistry: 2012; p 134–202.
- (13) Harhay, M. O.; Olliaro, P. L.; Costa, D. L.; Costa, C. H. N. Urban parasitology: visceral leishmaniasis in Brazil. *Trends Parasitol.* **2011**, *27* (9), 403–409.

- (14) De Rycker, M.; Hallyburton, I.; Thomas, J.; Campbell, L.; Wyllie, S.; Joshi, D.; Cameron, S.; Gilbert, I. H.; Wyatt, P. G.; Frearson, J. A.; Fairlamb, A. H.; Gray, D. W. Comparison of a high-throughput high-content intracellular leishmania donovani assay with an axenic amastigote assay. *Antimicrob. Agents Chemother.* **2013**, *57* (7), 2913–2922.

- (15) Don, R.; Ioset, J.-R. Screening strategies to identify new chemical diversity for drug development to treat kinetoplastid infections. *Parasitology* **2014**, *141* (1), 140–146.

- (16) Miles, T. J.; Thomas, M. G. Pyrazolo[3,4-d]pyrimidin Derivative and its use for the Treatment of Leishmaniasis. WO Patent WO2016116563A1, 2016.

- (17) Wyllie, S.; Thomas, M.; Patterson, S.; Crouch, S.; De Rycker, M.; Lowe, R.; Gresham, S.; Urbaniak, M. D.; Otto, T. D.; Stojanovski, L.; Simeons, F. R. C.; Manthri, S.; MacLean, L. M.; Zuccotto, F.; Homeyer, N.; Pflaumer, H.; Boesche, M.; Sastry, L.; Connolly, P.; Albrecht, S.; Berriman, M.; Drewes, G.; Gray, D. W.; Ghidelli-Disse, S.; Dixon, S.; Fiandor, J. M.; Wyatt, P. G.; Ferguson, M. A. J.; Fairlamb, A. H.; Miles, T. J.; Read, K. D.; Gilbert, I. H. Cyclin-dependent kinase 12 is a drug target for visceral leishmaniasis. *Nature* **2018**, *560* (7717), 192–197.

- (18) Woodland, A.; Grimaldi, R.; Luksch, T.; Cleghorn, L. A. T.; Ojo, K. K.; Van Voorhis, W. C.; Brenk, R.; Frearson, J. A.; Gilbert, I. H.; Wyatt, P. G. From on-target to off-target activity: identification and optimization of trypanosoma brucei GSK3 Inhibitors and their characterisation as anti-trypanosoma brucei drug discovery lead molecules. *ChemMedChem* **2013**, *8* (7), 1127–1137.

- (19) Ding, Q.; Jiang, N.; Roberts, J. L. Preparation of Pyrazolopyrimidines as Antitumor Agents. US Patent US20050277655A1, 2005.

- (20) Merritt, C.; Silva, L. E.; Tanner, A. L.; Stuart, K.; Pollastri, M. P. Kinases as druggable targets in trypanosomatid protozoan parasites. *Chem. Rev.* **2014**, *114* (22), 11280–11304.

- (21) Dichiaro, M.; Marrazzo, A.; Prezzavento, O.; Collina, S.; Rescifina, A.; Amata, E. Repurposing of human kinase Inhibitors in neglected protozoan diseases. *ChemMedChem* **2017**, *12* (16), 1235–1253.

- (22) Ferguson, F. M.; Gray, N. S. Kinase inhibitors: the road ahead. *Nat. Rev. Drug Discovery* **2018**, *17* (5), 353–377.

- (23) Hill, A. P.; Young, R. J. Getting physical in drug discovery: a contemporary perspective on solubility and hydrophobicity. *Drug Discovery Today* **2010**, *15* (15–16), 648–655.

- (24) Gupta, S.; Nishi. Visceral leishmaniasis: experimental models for drug discovery. *Indian J. Med. Res.* **2011**, *133*, 27–39.

- (25) Seifert, K.; Croft, S. L. In vitro and in vivo interactions between miltefosine and other antileishmanial drugs. *Antimicrob. Agents Chemother.* **2006**, *50* (1), 73–79.

- (26) Escobar, P.; Yardley, V.; Croft, S. L. Activities of hexadecylphosphocholine (miltefosine), AmBisome, and sodium stibogluconate (Pentostam) against leishmania donovani in immunodeficient scid mice. *Antimicrob. Agents Chemother.* **2001**, *45* (6), 1872–1875.

- (27) Dorlo, T. P. C.; Huitema, A. D. R.; Beijnen, J. H.; de Vries, P. J. Optimal dosing of miltefosine in children and adults with visceral leishmaniasis. *Antimicrob. Agents Chemother.* **2012**, *56* (7), 3864–3872.

- (28) Dorlo, T. P. C.; Rijal, S.; Ostyn, B.; de Vries, P. J.; Singh, R.; Bhattarai, N.; Uranw, S.; Dujardin, J.-C.; Boelaert, M.; Beijnen, J. H.; Huitema, A. D. R. Failure of miltefosine in visceral leishmaniasis is associated with low drug exposure. *J. Infect. Dis.* **2014**, *210* (1), 146–153.

- (29) Wyllie, S.; Patterson, S.; Stojanovski, L.; Simeons, F. R.; Norval, S.; Kime, R.; Read, K. D.; Fairlamb, A. H. The anti-trypanosome drug fexinidazole shows potential for treating visceral leishmaniasis. *Sci. Transl. Med.* **2012**, *4* (119), 119re1.

- (30) Bradley, D. J.; Kirkley, J. Regulation of leishmania populations within the host. I. the variable course of leishmania donovani infections in mice. *Clin. Exp. Immunol.* **1977**, *30* (1), 119–129.

- (31) Young, R. J.; Green, D. V. S.; Luscombe, C. N.; Hill, A. P. Getting physical in drug discovery II: the impact of chromatographic hydrophobicity measurements and aromaticity. *Drug Discovery Today* **2011**, *16* (17–18), 822–830.

(32) Klein, S. The use of biorelevant dissolution media to forecast the in vivo performance of a drug. *AAPS J.* **2010**, *12* (3), 397–406.

(33) Gilbert, I. H.; Thomas, M. G. Preparation of Antileishmanial Pyrazolopyrimidines. WO Patent WO2016116752A1, 2016.

(34) Di, L.; Fish, P. V.; Mano, T. Bridging solubility between drug discovery and development. *Drug Discovery Today* **2012**, *17* (9–10), 486–495.

(35) *The Sirius Gold Standard pKa Assays*; Pion, 2018; <http://www.sirius-analytical.com/analytical-services/gold-standard-assays> (accessed Aug 2, 2018).

(36) Jain, N.; Yalkowsky, S. H. Estimation of the aqueous solubility I: application to organic nonelectrolytes. *J. Pharm. Sci.* **2001**, *90* (2), 234–252.

(37) Young, R. J. Physical properties in drug design. *Topics in Medicinal Chemistry; Tactics in Contemporary Drug Design*, Springer: Berlin, Heidelberg, 2014; Vol. 9, pp 1–68, DOI: 10.1007/7355_2013_35.

(38) Ames, B. N.; McCann, J.; Yamasaki, E. Methods for detecting carcinogens and mutagens with the salmonella/mammalian-microsome mutagenicity test. *Mutat. Res.* **1975**, *31* (6), 347–364.

(39) Tao, H.; Santa Ana, D.; Guia, A.; Huang, M.; Ligutti, J.; Walker, G.; Sithiphong, K.; Chan, F.; Guoliang, T.; Zozulya, Z.; Saya, S.; Phimmachack, R.; Sie, C.; Yuan, J.; Wu, L.; Xu, J.; Ghetti, A. Automated tight seal electrophysiology for assessing the potential hERG liability of pharmaceutical compounds. *Assay Drug Dev. Technol.* **2004**, *2* (5), 497–506.

(40) Ly, J. Q.; Shyy, G.; Misner, D. L. Assessing hERG channel inhibition using PatchXpress. *JALA* **2005**, *10* (4), 225–230.

(41) Clive, D.; Johnson, K. O.; Spector, J. F.; Batson, A. G.; Brown, M. M. Validation and characterization of the L5178Y/TK± mouse lymphoma mutagen assay system. *Mutat. Res., Fundam. Mol. Mech. Mutagen.* **1979**, *59* (1), 61–108.

(42) Liu, T.; Brown, B. S.; Wu, Y.; Antzelevitch, C.; Kowey, P. R.; Yan, G.-X. Blinded validation of the isolated arterially perfused rabbit ventricular wedge in preclinical assessment of drug-induced proarrhythmias. *Heart Rhythm* **2006**, *3* (8), 948–956.

(43) Shah, R. R. Drug-induced QT interval shortening: potential harbinger of proarrhythmia and regulatory perspectives. *Br. J. Pharmacol.* **2010**, *159* (1), 58–69.

(44) Alvar, J.; Velez, I. D.; Bern, C.; Herrero, M.; Desjeux, P.; Cano, J.; Jannin, J.; den Boer, M. Leishmaniasis worldwide and global estimates of its incidence. *PLoS One* **2012**, *7* (5), No. e35671.

(45) Valko, K.; Bevan, C.; Reynolds, D. Chromatographic hydrophobicity index by fast-gradient RP-HPLC: a high-throughput alternative to Log P/log D. *Anal. Chem.* **1997**, *69* (11), 2022–2029.

(46) Wyllie, S.; Fairlamb, A. H. Refinement of techniques for the propagation of leishmania donovani in hamsters. *Acta Trop.* **2006**, *97* (3), 364–369.

(47) Sacks, D.; Sher, A. Evasion of innate immunity by parasitic protozoa. *Nat. Immunol.* **2002**, *3* (11), 1041–1047.